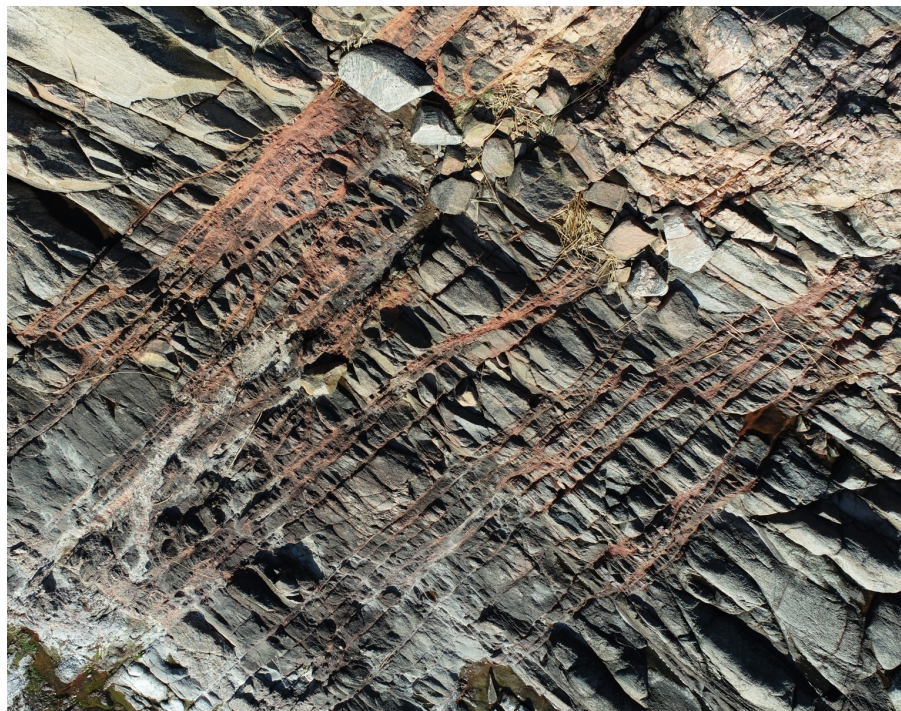


**Geological characterisation of
geophysical lineaments as part of the
expanded site descriptive model
around the planned repository site for
high-level nuclear waste, Forsmark,
Sweden**

Aron Bakker

Dissertations in Geology at Lund University,
Master's thesis, no 623
(45 hp/ECTS credits)



Department of Geology
Lund University
2021

**Geological characterisation of
geophysical lineaments as part of the
expanded site descriptive model
around the planned repository site
for high-level nuclear waste,
Forsmark, Sweden**

Master's thesis
Aron Bakker

Department of Geology
Lund University
2021

Contents

1 Introduction	7
2 Geological Setting	8
2.1 Large-scale lithotectonic framework	8
2.2 Bergslagen lithotectonic unit	10
2.3 Forsmark tectonic framework	10
2.3.1 Characterization of deformation zones	10
2.3.2 Fracture minerals and chemical alteration	12
2.4 Study area	12
3 Method	14
3.1 Expanded lineament model	14
3.2 Stage 1 field data collection: exploratory fieldwork	15
3.3 Stage 2 field data collection: detailed structural analysis	16
4 Results	16
4.1 NW-SE, WNW-ESE and NNW-SSE deformation zones	18
4.1.1 Coast between Öregrund and Stenskär	19
4.1.2 Central Gräsö	22
4.2 E-W (080-260 striking) deformation zones	31
5 Interpretation and Discussion	37
5.1 Deformation zone characteristics, kinematics, and fracture minerals	37
5.1.1 Splays from the Singö deformation zone	37
5.1.2 NW-SE and NNW-SSE striking deformation zones of central Gräsö	40
5.1.3 E-W (080-260) striking deformation zones	41
5.2 Tectonic development and paleostress reconstruction	42
5.3 Relationship between general structural grain and lineaments	44
6 Conclusions	46
7 Acknowledgments	46
8 References	47

Cover Picture: Aerial drone image of an extensional deformation zone on the west coast of Gräsö. Photo: Aron Bakker

Abstract

ARON BAKKER

Bakker, A., 2021: Geological characterisation of geophysical lineaments as part of the expanded site descriptive model around the planned repository site for high-level nuclear waste, Forsmark, Sweden . *Dissertations in Geology at Lund University*, No. 623, 48 pp. 45 hp (45 ECTS credits).

Abstract: The Swedish Nuclear Fuel and Waste Management Co. (SKB) started a project in 2020 near Forsmark, Sweden with the aim to expand the deformation zone model to encompass the entire catchment area around the planned repository for spent nuclear fuel. This thesis builds upon a lineament model that was constructed for SKB which utilizes airborne magnetic data supported by airborne Very Low Frequency (VLF) and elevation data. A selection of the lineaments was investigated in the field to verify whether or not they correspond to deformation zones, with a subsequent structural analysis for each confirmed deformation zone. My results show that NW-SE trending ductile deformation zones are characterized by a high degree of localized strain and are locally brittlely reactivated. These NW-SE trending deformation zones are found in areas inferred to previously have been affected by high ductile strain. The ductile deformation zones are interpreted to be splays from a regional-scale deformation zone which makes up the northern tectonic boundary of the so-called Forsmark tectonic lens and have tectonic precursors that developed during the 2.0-1.8 Ga Svecokarelian orogeny. Tens to hundreds of meters wide strongly red-stained brittle deformation zones are found on the island of Gräsö, located outside the higher ductile strain area. Locally, mylonitic fabrics in the cores of the zones are visible, indicating also here a ductile precursor to brittle deformation. E-W striking red-stained brittle deformation zones hosting a fracture mineral assemblage of calcite, adularia and laumontite are extensional in nature and are most likely related to the 1.1-0.9 Ga Sveconorwegian orogeny. Some lineaments in the northern parts of Gräsö that are oriented E-W and NW-SE are parallel to the gneissic banding of the host rocks and do probably not represent distinct deformation zones.

Keywords: Forsmark, deformation zones, Svecokarelian, Sveconorwegian, ductile-brittle transition, brittle deformation, mylonite

Supervisor(s): Susanne Grigull (SKB), Ulf Söderlund (LU), Jesper Petersson (SKB), Peter Hultgren (SKB).

Subject: Bedrock Geology

*Aron Bakker, Department of Geology, Lund University, Sölvegatan 12, SE-223 62 Lund, Sweden.
E-mail: ar7682ba-s@student.lu.se*

Sammanfattning

ARON BAKKER

Bakker, A., 2021: Geologisk karaktärisering av geofysiska lineament som del av den utvidgade platsbeskrivningen för planerat slutförvar för högaktivt radioaktivt avfall, Forsmark, Sverige. *Examensarbeten i geologi vid Lunds universitet*, Nr. 623, 48 sid. 45 hp.

Sammanfattning: Svenska Kärnbränslehanteringen (SKB) startade ett projekt under 2020 i närheten av Forsmark i Sverige med målet att utöka deformationszonsmodellen till att inkludera hela dräneringsområdet runt om det planerade slutförvaret för använt kärnbränsle. Detta arbete bygger på en lineamentmodell som var skapad för SKB. Denna modell använder sig av magnetiska data tillsammans med höjddata samt data insamlad med den flyggeofysiska Väldigt Låg Frekvens (VLF) metoden. Ett urval av lineamenten undersöktes i fält för att se om de stämmer överens med deformationszoner eller inte, och därefter gjordes en efterföljande strukturanalys för varje bekräftad deformationszon. Mina resultat visar att de nordväst-sydostgående duktila deformationszonerna karakteriseras av hög lokaliserad strain (resultat av stress) och är lokalt reaktiverade under spröda förhållanden. Dessa nordväst-sydostgående deformationszoner finns i områden som tidigare har blivit påverkade av hög duktil strain. De duktila deformationszonerna tolkas vara 'splays' som viker av från en deformationszon av regional storlek som utgör den norra tektoniska gränsen av den så kallade Forsmark tektoniska linsen och har tektoniska föregångare som bildades under den Svekokarelska orogenesisen (2,0-1,8 miljarder år sedan). På Gräsö finns tiotals till hundratals meter breda, starkt rödfärgade spröda deformationszoner utanför det högre duktila strainområdet. Lokalt ses mylonit i de inre delarna av dessa deformationszoner som även här tyder duktil deformation före den spröda deformationen. Öst-västliga rödfärgade spröda deformationszoner med sprickmineralerna kalcit, adularia och laumontit är extensionella och förmodligen kopplade till den Svekonorvegiska orogenen (1,1-0,9 miljarder år sedan). Några av lineamenten i den norra delen av Gräsö som sträcker sig öst-väst och nordväst-sydost är parallella med den gnejsiga bandningen och representerar förmodligen inte distinkta deformationszoner.

Nyckelord: Forsmark, deformationzoner, Svekokarelska, Sveconorvegiska, duktila-spröda övergången, spröd deformation, mylonit

Handledare: Susanne Grigull (SKB), Ulf Söderlund (LU), Jesper Petersson (SKB), Peter Hultgren (SKB).

Ämnesinriktning: Berggrundsgeologi

Aron Bakker, Geologiska institutionen, Lunds Universitet, Sölvegatan 12, 223 62 Lund, Sverige.

E-post: ar7682ba-s@student.lu.se

1 Introduction

The Swedish Nuclear Fuel and Waste Management Co (SKB) is planning to build a geological repository for spent nuclear fuel at about 500 m depth in the bedrock near Forsmark, Sweden (Fig. 1.1) according to the so-called KBS-3 method. In general terms, the KBS-3 concept consists of a cast iron insert with the spent fuel encapsulated in copper canisters, surrounded by a bentonite clay buffer, to be placed in deposition holes in the bedrock. This method has been developed over several decades during which extensive research into both the technical barriers and the bedrock barrier has been performed in order to fulfil the requirements of short- and long-term safety for the planned repository (SKB 2011).

Currently, only low- and medium level nuclear waste is stored at Forsmark in the Final Repository for Short-Lived Radioactive Waste (SFR), a facility located at about 60 m depth beneath the sea floor. The spent nuclear fuel, classified as high-level radioactive waste, currently rests in an interim repository called Clab in Simpevarp, about 25 km north of Oskarshamn, southeastern Sweden.

Based on extensive site investigations performed at Forsmark a so-called site descriptive model (SDM) was developed and is updated regularly. The SDM integrates geology, rock mechanics, thermal

properties, hydrogeology, hydrogeochemistry, transport properties and the surface system. Both the repository layout design as well as the research into pre- and post-closure safety depend on the SDM. As part of the geological modelling for the SDM, a deterministic deformation zone model has been developed based on surface observations, borehole interpretations and the interpretation of geophysical lineaments and seismic reflectors. Modelling was done for certain model volumes on a so-called regional and a local scale, which differ in extent for the planned spent fuel repository and the SFR-facility (Fig. 1.1) The regional models extend to 2100 m depth for the planned repository and to 1100 m for the SFR-facility. The most-recent version of the local and regional deterministic deformation zone models for the spent fuel repository is presented in Stephens & Simeonov (2015). The model by Stephens & Simeonov (2015) also takes into account the deformation zone model by Curtis et al. (2011) developed for the SFR-facility.

As part of their ongoing geological and hydrogeological research, SKB is currently expanding the deformation zone model (Forsmark version 2.3) to include the entire catchment area surrounding the planned nuclear waste repository. The catchment area defined as the future maximum area where precipitation collects and runs off into a body of water (Fig. 1.2). This maximum catchment area is an

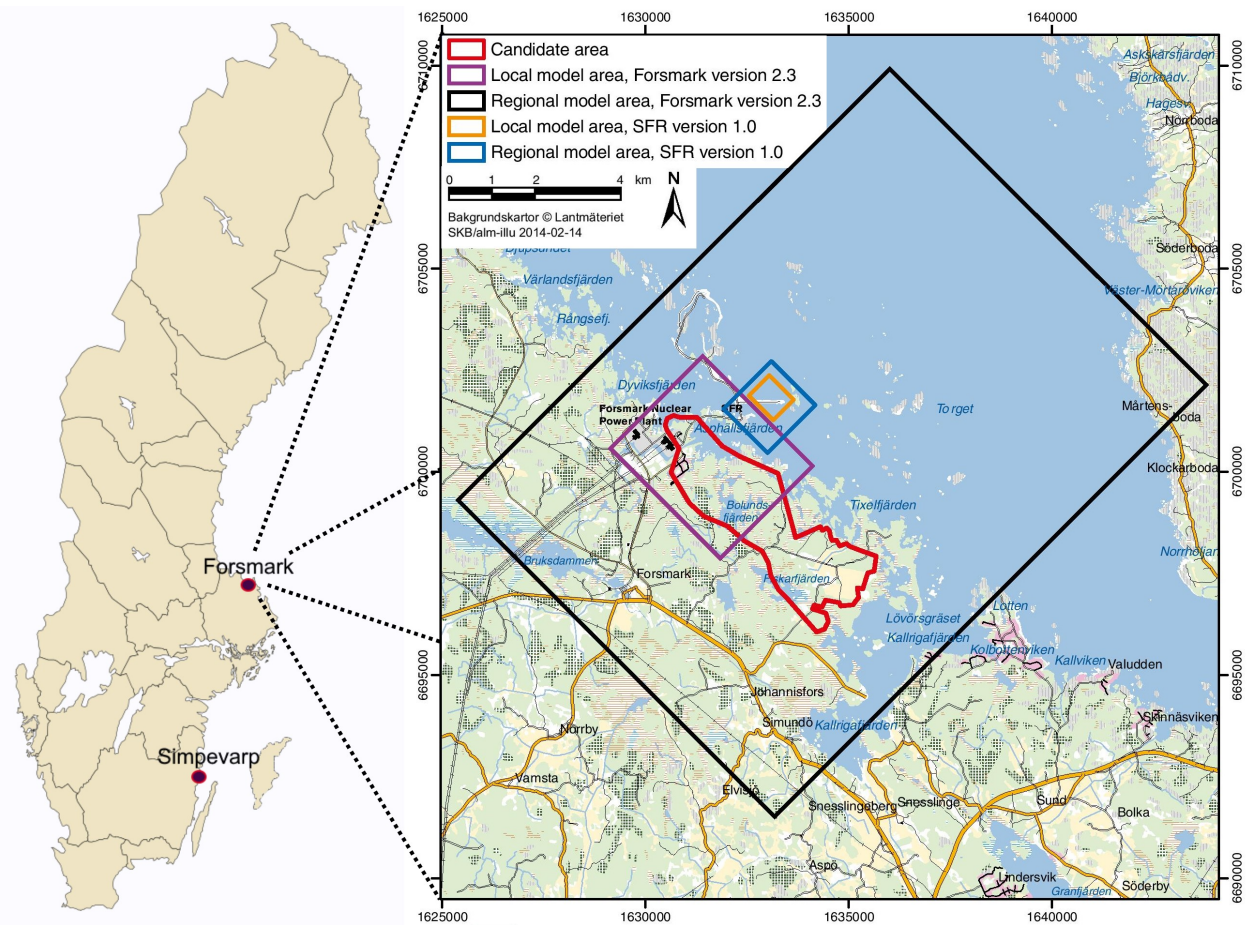


Fig. 1.1. Left: location of the Forsmark research area and interim storage facility Simpevarp (Southeast Sweden). Right: details of the Forsmark area pictured with the outlines of all current model areas (From Stephens & Simeonov (2015)). Currently, the largest model area (black rectangle) is the regional model area for the planned spent fuel repository. The blue and orange rectangles represent the regional and local model areas for the low- and medium-level nuclear waste repository (SFR), respectively.

important perimeter as it is used in hydraulic flow modelling in bedrock, as input to the long term safety assessment of the spent nuclear fuel storage. The hydraulic flow models will be based on Discrete Fracture Network (DFN) modelling, which in turn is primarily based on the deterministic deformation zone model of the catchment area. The update of the deformation zone model is based on an extended lineament study by Isaksson & Johansson (2020) and is currently revised by Petersson & Hultgren (2021, in prep.).

Knowledge of deformation zones and fractures are critical for hydrogeological modelling since they directly affect the groundwater flow as well as the mechanical stability of the rock mass (SKB 2011). The overall objective of this thesis is to provide confidence for the modelled deformation zones by means of geological field work, during which the characteristics and extent of deformation zones in the expanded model area are documented and investigated. The study is based on the lineament interpretation by Isaksson & Johansson (2020) (see chapter 3) and is placed within the context of existing structural models of the smaller regional area. More specifically, the main research question of this study is whether the deformation zones observed in the expanded work area can be linked to the existing deformation zone model described in Stephens & Simeonov (2015) and explained by the existing model for the tectonic evolution of Forsmark (Saintot et al. 2011, Stephens et al. 2015). The results of this thesis provide input for a broader regional structural model.

2 Geological background

Most of the information summarised in sections 2.1 and 2.2 is taken from the recently published book ‘Sweden: Lithotectonic Framework, Tectonic Evolution and Mineral Resources’, edited by M.B. Stephens and J. Bergman Weihed (2020), and references therein.

2.1 Large-scale lithotectonic framework

The Swedish bedrock is part of the Fennoscandian Shield (Fig. 2.1) and the vast majority of the rocks are Proterozoic and Archean in age. Proterozoic orogenesis has affected these rocks to various degrees and at different times, and the most prominent one is the so-called 2.0 – 1.8 Ga Svecofennian orogeny as it affects more than half of the Paleoproterozoic and Archean rocks in Sweden (Fig. 2.1; e.g. Stephens 2020).

Sweden can be subdivided into six lithotectonic units, most of them bound by deformation zones (Stephens & Bergman 2020 and references therein). Forsmark lies in the north-eastern part of one of these units called the Bergslagen lithotectonic unit (Fig. 2.2), known for its mineral resources (Stephens & Jansson 2020). The Bergslagen lithotectonic unit is truncated by several NW-SE striking shear zones in the north-eastern part (Stephens & Bergman 2020) (Fig. 2.2).

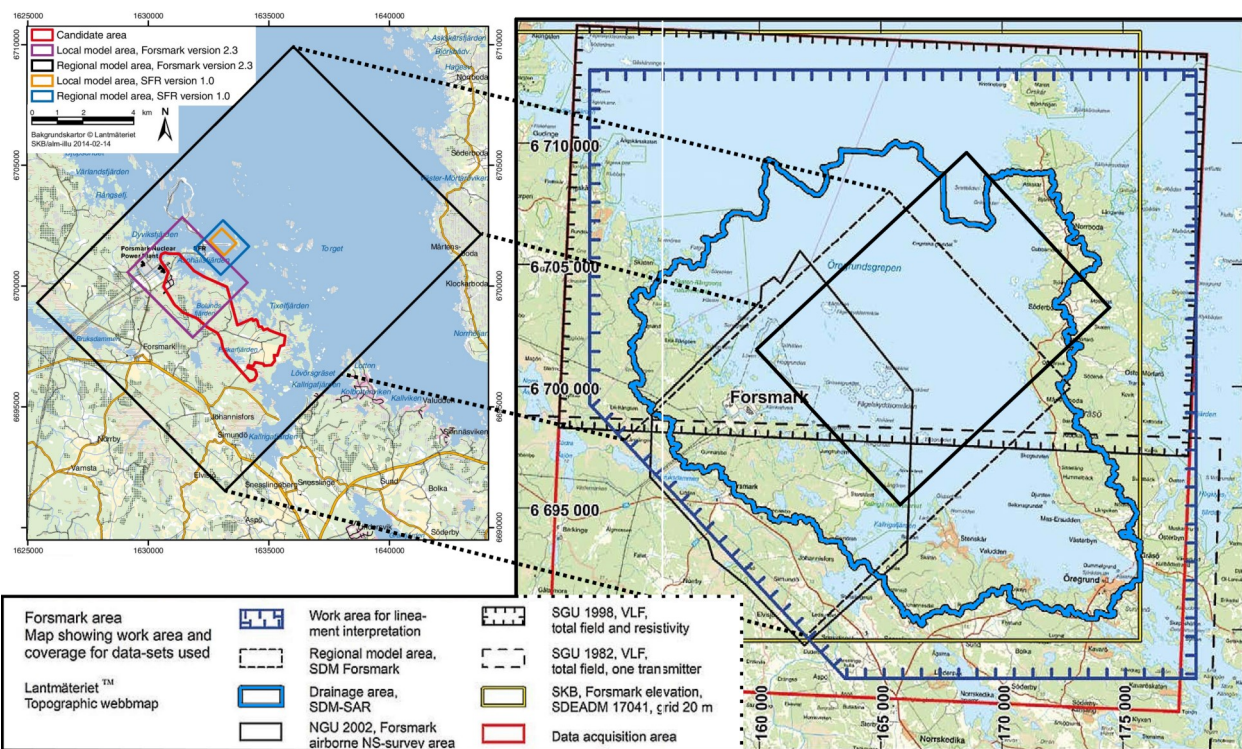


Fig. 1.2. Left: Extent of the regional and local model areas at Forsmark. Right: Coverage of data-sets used by Isaksson & Johansson (2020) as base for lineament interpretation. The light blue outline in the right map represents the future maximum catchment area and the dark blue outline with perpendicular dashes represents the total work area for the lineament interpretation by Isaksson & Johansson (2020) which coincides with the study area of this MSc-project.

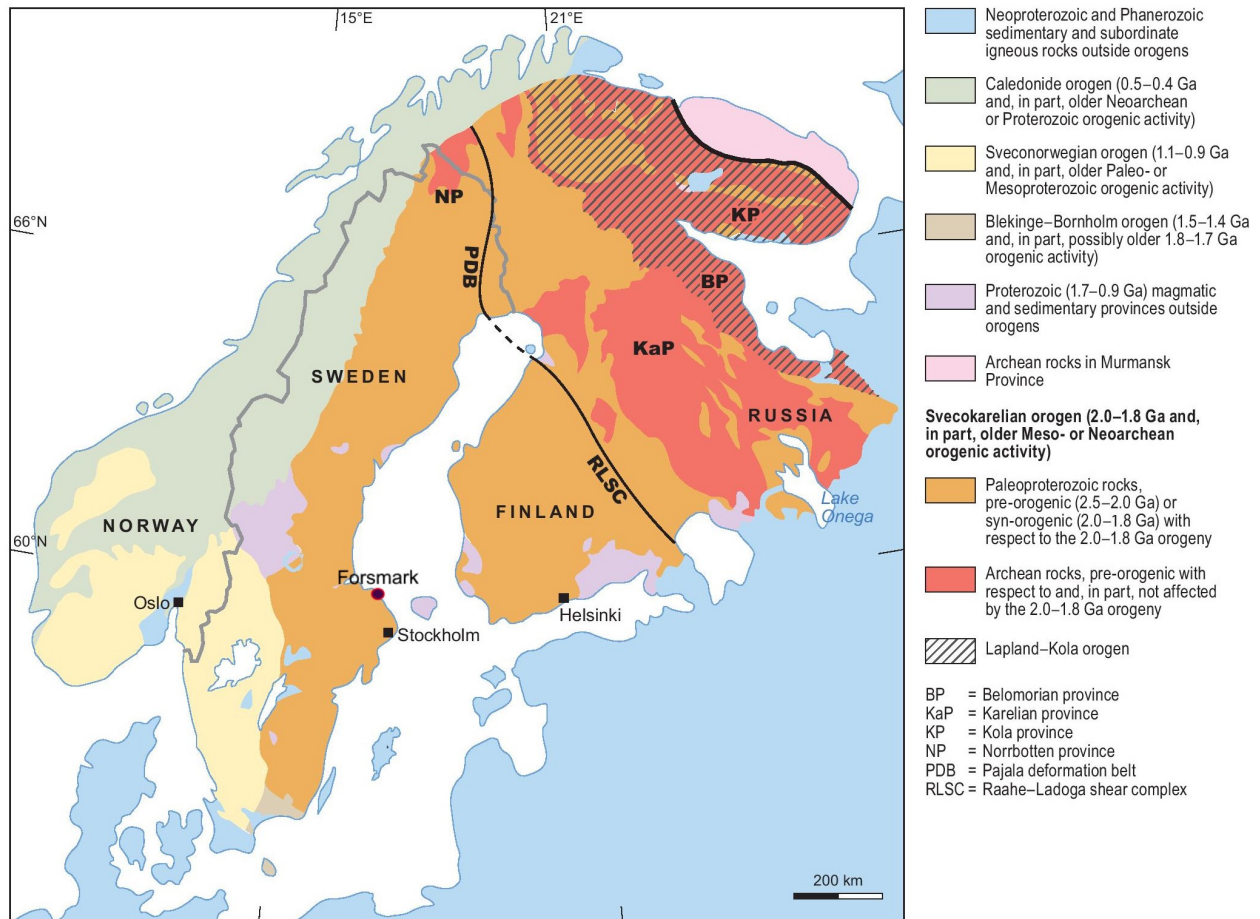


Fig. 2.1. Map of the major lithotectonic units of Norway, Sweden and Finland (Stephens & Bergman 2020, modified after Koistinen et al. 2001). The work area near Forsmark is indicated.

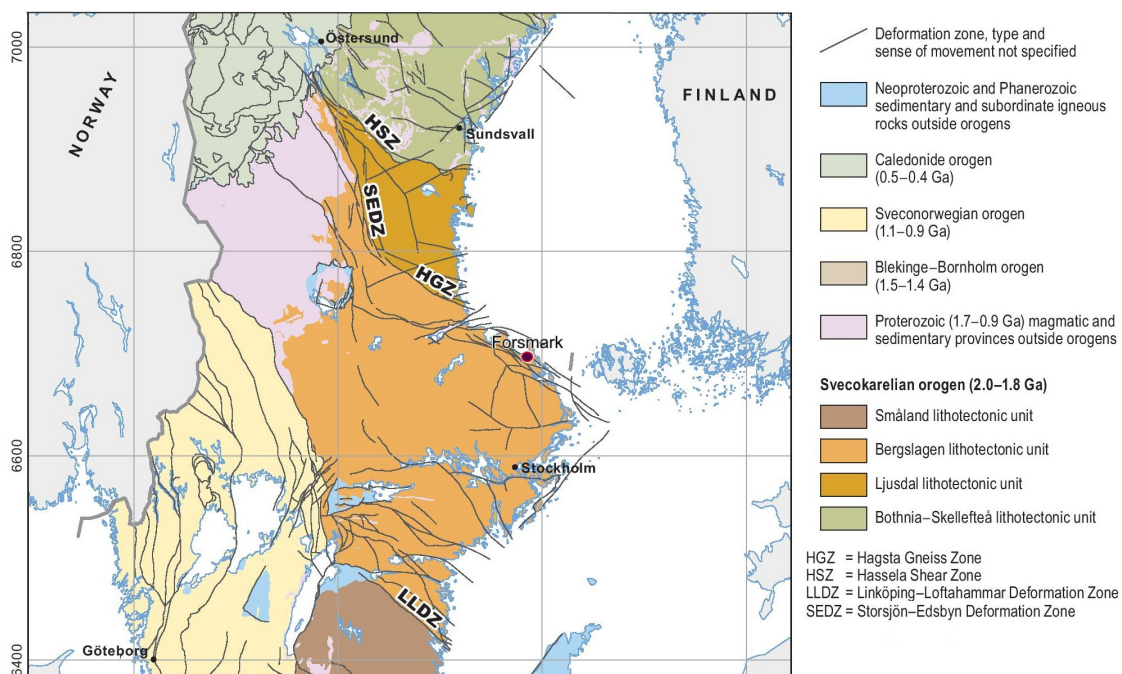


Fig. 2.2. Detail of the lithotectonic units in Sweden between the Hassela Shear Zone (HSZ) and Loftahammar-Linköping Deformation Zone (LLDZ), modified from Stephens & Bergman (2020). The work area around Forsmark is labelled, situated in the Bergslagen lithotectonic unit.

2.2 Bergslagen lithotectonic unit

The rocks that make up the Bergslagen lithotectonic unit are mostly meta-granitoids (granites, granodiorites and tonalites, see also Fig. 2.6) with few metamorphosed diorites, gabbros, ultramafic rocks and felsic volcanic rocks (Bergman et al. 2012; Stephens & Jansson 2020). The majority of the unit consists of rocks formed as a result of magmatic activity at c. 1.87-1.84 Ga and c. 1.81-1.78 Ga (Stephens & Jansson 2020). Early development of planar and linear fabrics started around 1.87 Ga, induced by stress and heating from magmatic activity during orogenesis (Stephens & Jansson 2020).

Three Svecofennian tectonic cycles affected the Bergslagen lithotectonic unit and took place between 1.91 and 1.75 Ga, with each cycle lasting about 50-55 million years (Stephens & Jansson 2020; Stephens 2020). These cycles consist of alternating crustal shortening and extensional events, attributed to subduction hinge advance and retreat respectively (Hermansson et al. 2008a). The direction of subduction was to the northeast, beneath an active continental margin (Hermansson et al. 2008a; Stephens et al. 2009). During these events, the rocks in the northern and southern part of the Bergslagen lithotectonic unit were subjected to upper amphibolite and locally granulite-facies metamorphism at relatively low pressure and high temperature conditions (Stephens & Jansson 2020). During each of these tectonic cycles, distinctive deformation occurred in the ductile regime. After the first development of planar and linear fabrics, these structures were sheared and folded during each transpressional event (Högdahl et al. 2009; Stephens et al. 2009; Beunk & Kuipers 2012; Kampmann et al. 2016; Jansson 2017; Jansson et al. 2017).

2.3 Forsmark tectonic framework

2.3.1 Characterization of deformation zones

Among the three tectonic cycles that have affected the Bergslagen unit, two can be identified in the Forsmark region (Hermansson et al. 2007; Hermansson et al. 2008a). Locally at Forsmark, ductile deformation started at 1.87 Ga (Hermansson et al. 2008b), resulting in the formation of WNW-ESE or NW-SE trending strongly banded shear belts (Stephens & Jansson 2020). These high-strain shear belts are visible as the polka-dotted area in figure 2.3 (Saintot et al. 2011, modified after Stephens et al. 2007). After cooling below the 500° geotherm around 1.8 Ga, deformation under lower amphibolite to upper greenschist facies continued along discrete shear zones (Hermansson et al. 2008b; Saintot et al. 2011). The shear zones are anastomosing in nature and envelop so-called tectonic lenses, three-dimensional volumes of bedrock which show subordinate internal deformation (Stephens et al. 2009). The tectonic lenses were affected by regional scale tubular folding in a deformation event before the origin of the discrete shear zones and are eye-shaped at the current erosional level (Stephens et al. 2009; Stephens & Jansson 2020). There are three discrete shear zones surrounding the Forsmark tectonic lens which will host the planned high-level waste

repository, namely the ~180 m wide and >35 km long Singö deformation zone in the north, the ~140 m wide and ~70 km long Forsmark deformation zone in the south and the ~20-50 m wide and ~17 km long Eckarfjärden deformation zone in the middle (Stephens & Simeonov, 2015) (Fig. 2.3).

The deformation zones were first identified from airborne magnetic survey data (E-W data: Geological survey of Sweden, SGU; N-S data: Geological survey of Norway, NGU) where they show magnetic minima on the ground surface, and later confirmed with cored borehole data. The major steeply dipping Singö, Forsmark and Eckarfjärden deformation zones are visible as wide magnetic minima (Isaksson & Keisu 2005; Isaksson et al. 2007), striking WNW-ESE (Singö and Forsmark DZ) and NW-SE (Eckarfjärden DZ). In the context of the Svecofennian orogeny, the Singö and Forsmark deformation zones are the main shear zones and the Eckarfjärden deformation zone is interpreted as a Riedel shear zone in between (Saintot et al. 2011; Stephens et al. 2015). Smaller deformation zones striking ENE-WSW and NNE-SSW within the Forsmark tectonic lens are also visible as magnetic lows in the magnetic survey maps. The low magnetic reading is interpreted to be related to either pegmatitic dykes which by nature have a low magnetic susceptibility (Stephens et al. 2015), or to hydrothermal alteration of fracture minerals found in steeply dipping brittle deformation zones and hydrothermal alteration of the wall rock (Sandström et al. 2008; Stephens et al. 2015). Magnetic minima can also be seen between boundaries of different rock types, where the low magnetic signature is parallel (concordant) to the foliation (Stephens et al. 2015). Sandström et al. (2008) states that the bedrock in the regional model area is affected by hydrothermal alteration, mainly replacement of magnetite to hematite. Hematite stains fractures resulting in a red colour of both the actual fracture minerals and locally also a red-stained halo can be seen along the fractures in the host rock (Sandström et al. 2008). This oxidation halo is typical for the vast majority of the zones at Forsmark and is the basis for the connection between deformation zones and magnetic lows. From subsequent observations, deformation zones can be classified on the basis of ductility, brittleness, strike, and shear sense. Dating of fracture minerals often provides a minimum age of the formation of the fractures, which is helpful in constraining relative ages of deformation events.

A model for the characteristics and spatial variability of deformation zones and their evolution through time in the Forsmark regional area is depicted in figure 2.4 (Saintot et al. 2011; Stephens et al. 2015). In the simplified model (Fig. 2.4), the Singö, Forsmark, and Eckarfjärden deformation zones are interpreted to have formed under retrograde lower amphibolite- to greenschist metamorphic conditions under roughly N-S oriented horizontal compression between 1.85 and 1.8 Ga. After 1.8 Ga, transition into a colder regime caused ductile-brittle and brittle reactivation under the same stress field and formation of new Riedel shears (Fig. 2.4a). During a 1.7 – 1.6 Ga transpressional event, the stress field was directed approximately NE-SW and caused sinistral brittle

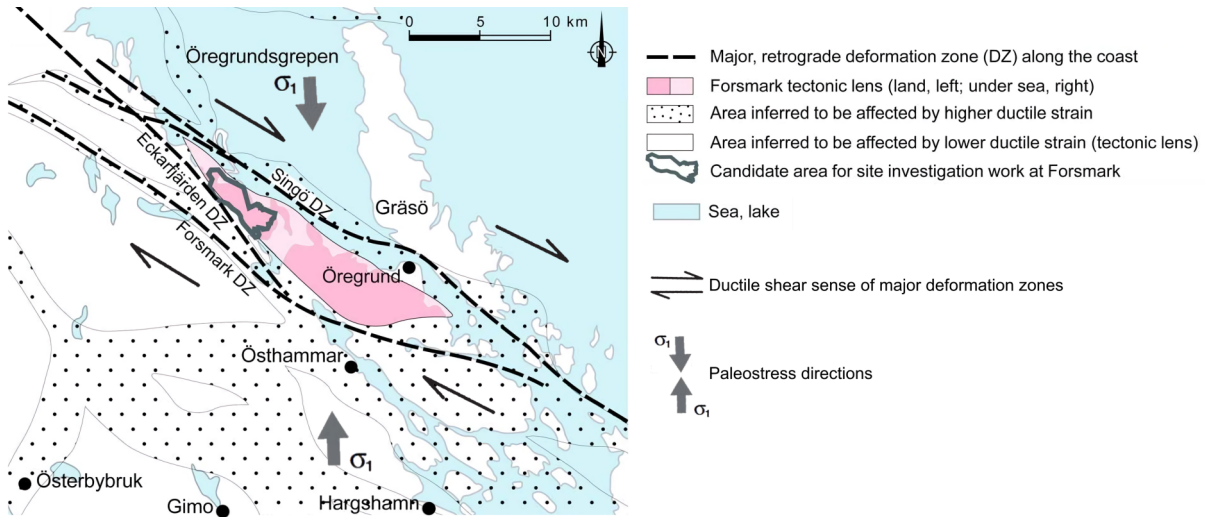


Fig. 2.2.. Detail of the Forsmark tectonic lens (pink shaded area) with its surrounding three major deformation zones (Saintot et al. 2011, modified after Stephens et al. 2007), shaped by the Sveco-karelian orogen under roughly N-S transpression at ca. 1.8 Ga (Stephens et al. 2015). Ductile shear sense markers are taken from Stephens & Jansson (2020). Paleostress directions and markers are taken from Stephens et al. (2015). ‘Eye-shaped’ tectonic lenses are situated between NW-SE high-strain deformational belts, which under a N-S oriented maximum horizontal stress have an inferred dextral shear component.

reactivation of the deformation zones formed during the Sveco-karelian orogeny (Fig. 2.4b). During the 1.1 – 0.9 Ga Sveconorwegian orogeny, further sinistral brittle reactivation occurred (Fig. 2.4c, Stephens et al. 2015).

Stephens et al. (2015) group deformation zones primarily according to their dip and strike: vertical or steeply dipping deformation zones trending WNW-ESE or NW-SE and deformation zones that trend ENE

-WSW or NNE-SSW differ in characteristics. The WNW-ESE and NW-SE deformation zones (like the Singö, Forsmark and Eckarfjärden DZ’s) comprise both ductile and brittle deformation and have a (proto) mylonitic, cataclastic and cohesive breccia fault core. The ENE-WSW and NNE-SSW striking zones accommodate brittle deformation with a fault core consisting of a highly elevated fracture frequency, locally with a cohesive breccia or cataclasis.

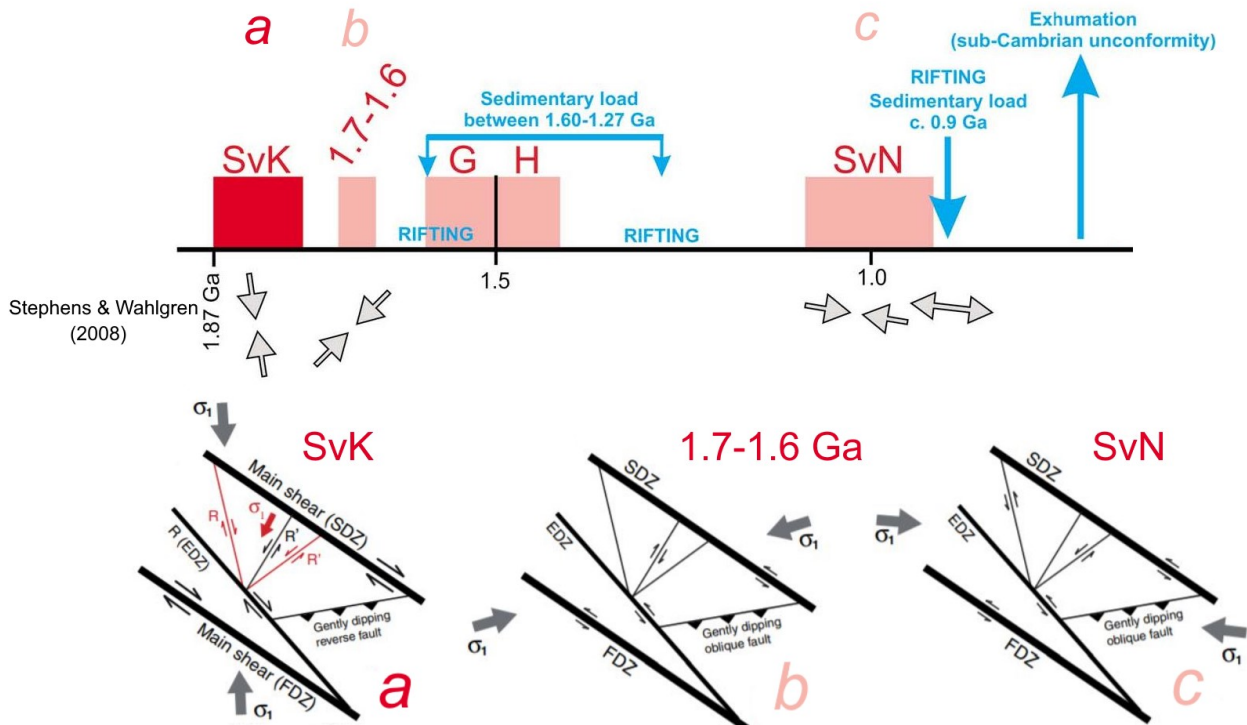


Fig. 2.4. Timeline of orogenic events affecting deformation- and fracture zones locally at Forsmark. Main stress component (σ_1) directions and the simplified model for fracture direction and strike-slip shear sense during a) The Sveco-karelian orogeny, with a clockwise-rotated stress field between the SDZ and EDZ resulting in the formation of NNW-SSE and NE-SW Riedel deformation zones b) The 1.7 – 1.6 Ga orogeny and c) the Sveconorwegian orogeny should be interpreted as viewed from above with the top of the model representing north. These schematic models are taken from Saintot et al. (2011) and Stephens et al. (2015). Timeline for these events is taken from Saintot et al. (2011).

As the principle stress directions varied over time, the main shear zones and their accompanying Riedel shear show strike-slip displacement with both dextral and sinistral sense of shear (Fig. 2.4).

2.3.2 Fracture minerals and chemical alteration

Fractures throughout the regional area around Forsmark can be distinguished based on the fracture minerals, making up four generations in total (Sandström et al. 2006). In this project, only the first and second generation of fracture minerals will be addressed, since they are associated with the characteristic red-staining of fracture minerals and the host rock along these fractures (Sandström et al. 2009: see inset figure in 2.5). The first generation is characterized by an assemblage of epidote, quartz and chlorite and is argued to be precipitated during the waning stages of the Sveconorwegian orogeny in a ductile-brittle transitional regime (Söderlund et al. 2008; Sandström et al. 2009). These minerals are typically found in gently-dipping fractures or steep NW-SE to WNW-ESE fractures (Sandström et al. 2009). The second generation of fracture minerals is constrained to the early Sveconorwegian orogeny, between 1.1 and 1.0 Ga (Sandström et al. 2009). It consists of a mineral paragenesis of hematite-stained adularia, albite, laumontite, and non-stained calcite, chlorite and prehnite. A timeline of fracture mineral generations is depicted in figure 2.5.

The characteristic red-staining of fracture minerals and the host rock around the fractures (halo's) observed throughout the Forsmark tectonic area is a result of hydrothermal activity: magnetite in altered grains is replaced by hematite (Sandström et al. 2008).

The halo that forms in the surrounding rock is a result of the replacement of magnetite by hematite and the fine dispersion of sub-microscopic hematite (Sandström et al. 2008). With a high density of fractures follows a high density of hematite, which lowers the magnetic susceptibility of the bedrock. These anomalies form the basis of lineaments derived from airborne magnetic data.

2.4 Study area

The work area where Isaksson & Johansson (2020) performed their lineament interpretation (Figs. 1.2 and 2.6) envelops the catchment area outside the Forsmark regional model area. The land area consists of the island Gräsö, and the coastal area from Öregrund to the northwestern shore of the Öregrundsgrepen (Fig. 2.6). The land area west of the settlement Stenskär is not considered in this project, as that is already part of the regional site descriptive model (Fig. 1.1, Fig. 1.2). The excluded area is shaded blue in figure 2.6. The area within the expanded model that is covered by the Baltic Sea or any other body of water is also not discussed in this thesis.

From the geological map of figure 2.6, the main types of bedrock are discerned based on their age and protolith, and all are classified as 'gnejsiga bergarter' which translates to 'gneissic rock types'. The bedrock of Gräsö is divided in quartz and feldspar-rich (granitic) gneisses in the north (Fig. 2.7a) and gneissic granitoids in the south (Fig. 2.7b). The contact between these two rock types as well as the ductile deformation zone near it strike NW-SE.

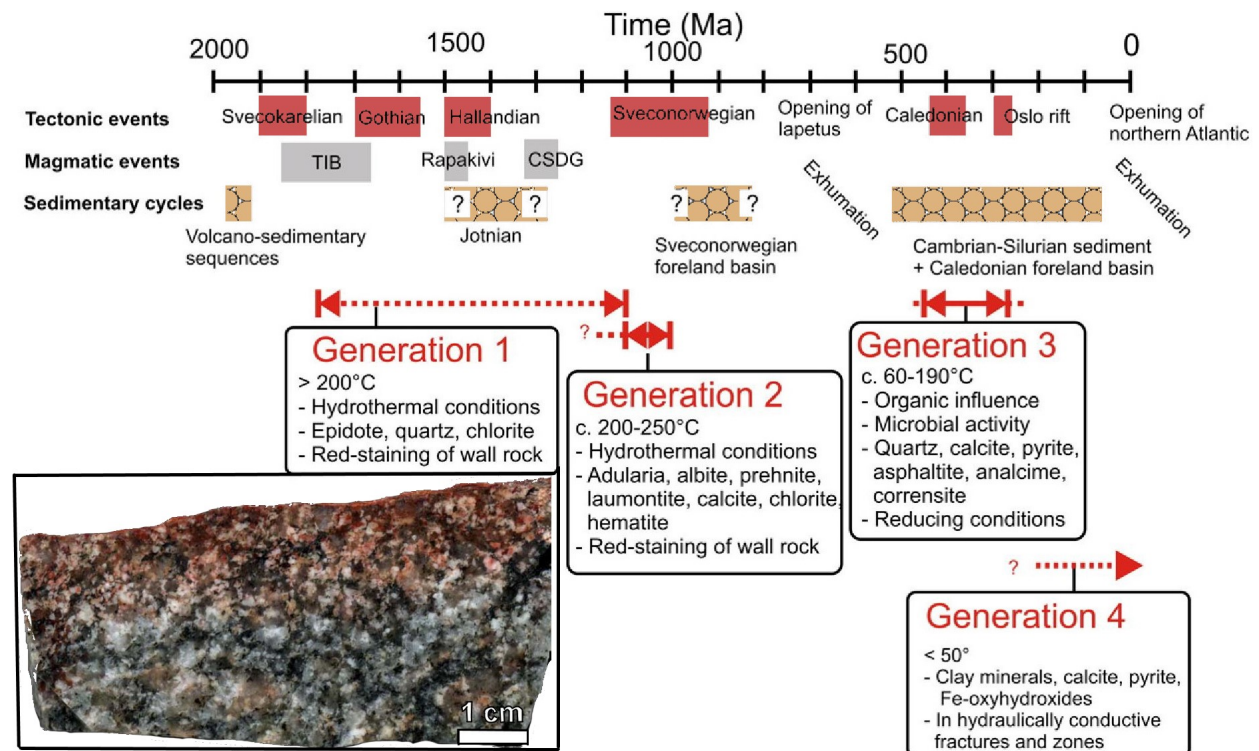


Fig. 2.5. Generations of fracture minerals modified from Sandström et al. (2009). Generation 1 and 2 mineral parageneses are associated with red-staining of wall rock. Bottom left: example of red-staining 'halo' feature penetrating c. 1.5 cm into the host granitoid rock from the generation 2 fracture (laumontite-sealed) seen in the upper part of the rock, modified from Sandström et al. (2008).

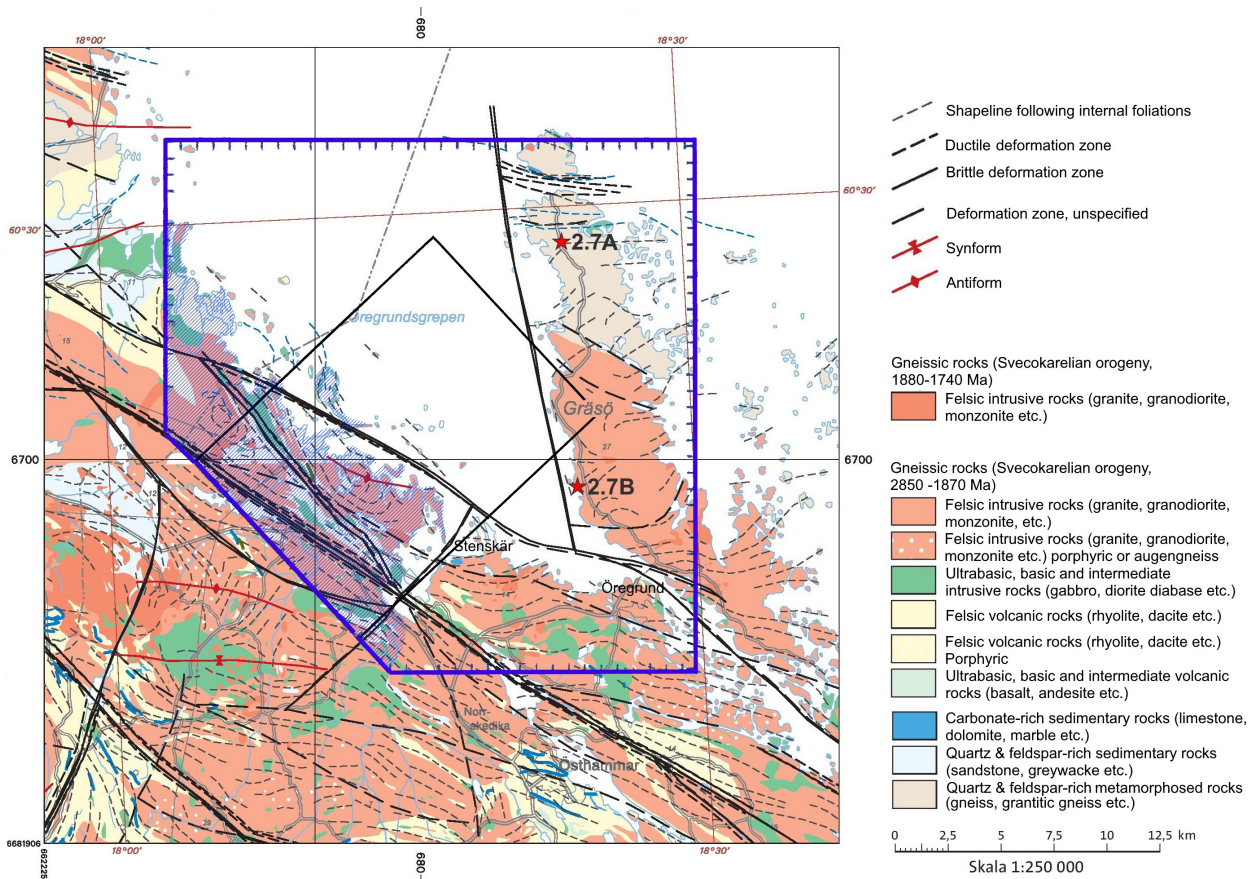


Fig. 2.6. Geological map from the Swedish Geological Survey (SGU), with an original scale of 1:250000. Black rectangle represents the extent of the regional model area. Blue line with perpendicular dashes represents the work area for lineament interpretation by Isaksson & Johansson (2020). Blue shaded area represents land area not studied for lineament interpretation in this project. Red stars represent locations of a typical gneiss (Fig. 2.7a) and gneissic granitoid (Fig. 2.7b).

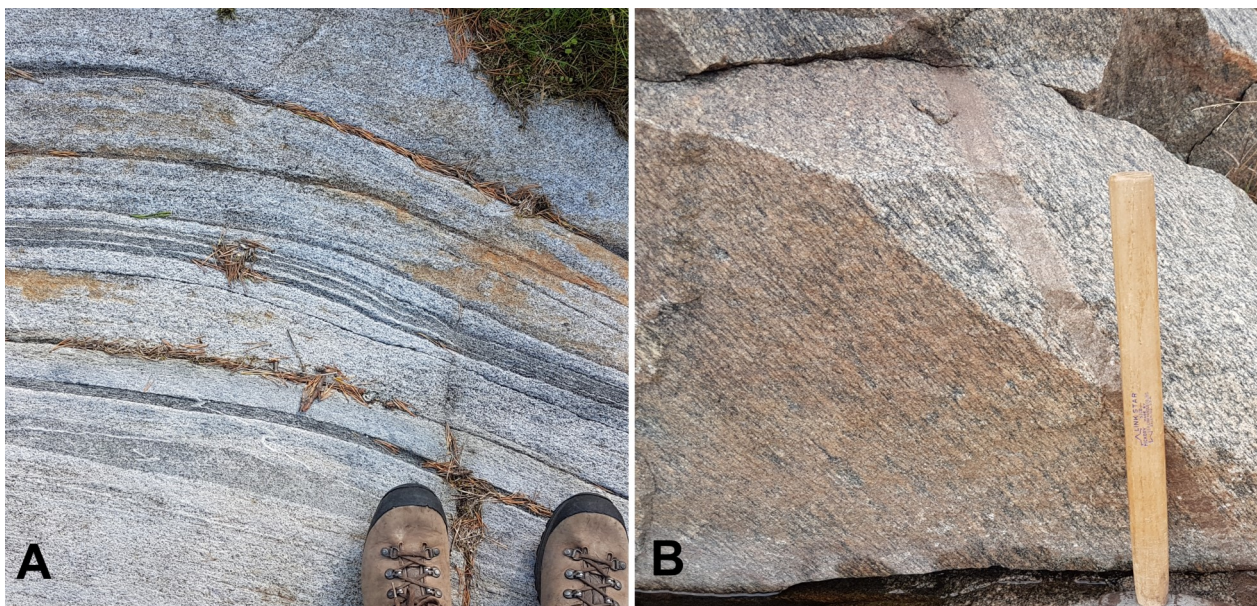


Fig. 2.7. **A.** Typical banded gneiss found in the northern part of Gräsö. **B.** Typical gneissic granite found in the southern part of Gräsö.

3 Method

3.1 Expanded lineament model

For this study, geological field work was performed to verify and characterise geophysical lineaments in the expanded regional model area. The lineament interpretation was done by Isaksson & Johansson (2020) and is mostly based on magnetic anomaly surveys, with support of Very Low Frequency (VLF) survey data and elevation data. The VLF method is used by geophysicists to detect water bearing zones: water has a higher conductivity and lower resistivity than the surrounding crystalline rock. The geological field work for this study is divided into two stages: a first stage including field work for verification of lineaments as major deformation zones and a second stage during which outcrops of the verified lineaments (deformation zones) are revisited and investigated in more detail.

The first lineament map was constructed for SKB by Geovista AB (Isaksson & Johansson, SKB report P-20-14) in April 2020 and its implementation in the work map used for the first field work stage is shown in figure 3.1. This work map is an early deformation zone investigation made by Petersson & Hultgren (SKB 2020).

It is important to note that in this first lineament model all geological interpretations were based on geophysical data and data from an older site descriptive model of Forsmark (version 2.3, Stephens

& Simeonov 2015), with no field observations in the expanded area.

Not all lineaments had the same degree of certainty: for example, a lineament that is clearly visible from airborne magnetic maps may not be supported by VLF and topographical data. Therefore, a weight number from 1 to 5 was attributed to each lineament, where a score of 1 means a very low degree of confidence and a score of 5 meaning a very high degree of confidence (Isaksson & Johansson 2020, based on methodology of Andersson (2003) and Isaksson & Keisu (2005)). A total of fifty new lineaments with a minimum ground surface trace length of 3 kilometres have been interpreted (Isaksson & Johansson 2020). As a continuation of the smaller site descriptive model, some new lineaments were linked to lineaments documented in previous reports.

The following low-altitude (<60 m ground clearance) airborne geophysical surveys formed the basis for the first lineament model by Isaksson & Johansson (2020) (Table 3.1).

All available data described in the table have been processed and compiled in report P-20-14 by Isaksson & Johansson (2020), resulting in the lineament interpretation. They mention that rocks with intense and penetrative ductile foliation cause a banded pattern in magnetic properties, making it hard to discern discrete deformation zones.

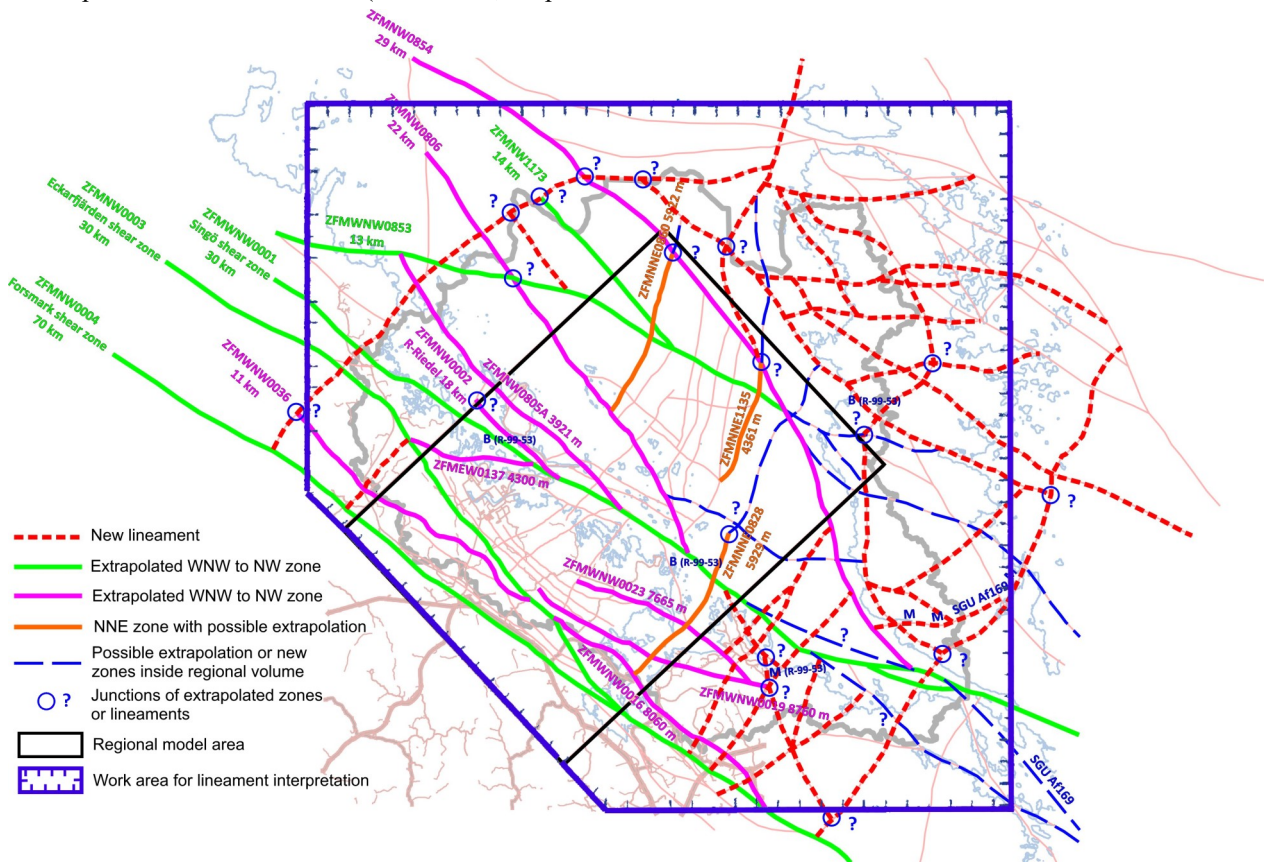


Fig. 3.1. Work map showing previously known deformation zones linked to interpreted lineaments (possible new deformation zones) derived from the report by Isaksson & Johansson (2020).

1	An aggregation of the various airborne measurements from 1977 – 1998 (SGU), with a transformation of measurement from 30 m ground clearance to a common measurement plane of 60 m above ground (Bergman et al. 1999).
2	Magnetic data from 2019 (SGU).
3	High-resolution magnetic grid data from the Forsmark survey 2002 (Stephens et al. 2007).
4	VLF total field (40 x 200 m grid, one transmitter) from the pre-study Östhammar regional survey (Bergman et al. 1996).
5	VLF total field and resistivity data (two transmitters) from the 1998 SGU regional survey.
6	Elevation data (20 x 20 m seafloor grid, 1 x 1 m land grid), provided by SKB.
7	Elevation data (50 x 50 m grid) from Lantmäteriet (open data).

Table 3.1 Seven datasets used by Isaksson & Johansson (2020) to construct the first lineament model for the expanded site description model area.

3.2 Stage 1 field data collection: exploratory fieldwork

Each new lineament, where possible, was visited in at least one locality during stage 1 of this project (late September to early October 2020). For each locality, GPS coordinates (SWEREF 99 TM 18 00 grid) and a brief geological description have been documented including a brief interpretation. Attitudes are given in strike/dip using the right-hand-rule (RHR). In some cases, no viable outcrops were found near the lineament. Deformation zones that were discovered without any link to a lineament were also noted. The majority of outcrops on Gräsö and between Öregrund and Stenskär were investigated on well-exposed, coastal outcrops that are free from vegetation overgrowth.

After the stage 1 field data collection, the lineament model from Isaksson & Johansson (2020) was reassessed by Petersson & Hultgren (2021 in prep.) and changes were implemented (Fig. 3.2) The lower limit for deformation zones to be included in the new model was set to be 5 km. The new lines depicted in figure 3.2 are not lineaments in the strict sense, but rather deformation zone line traces. To keep consistency throughout this project, the line traces are still referred to as lineaments. The relation between the magnetic anomaly map from SGU and the modelled zones for the expanded work area is shown in figure 3.3. The resolution of the magnetic field data for the expanded model area is significantly lower than in the regional model area of Forsmark, version 2.3 (Stephens & Simeonov 2015).

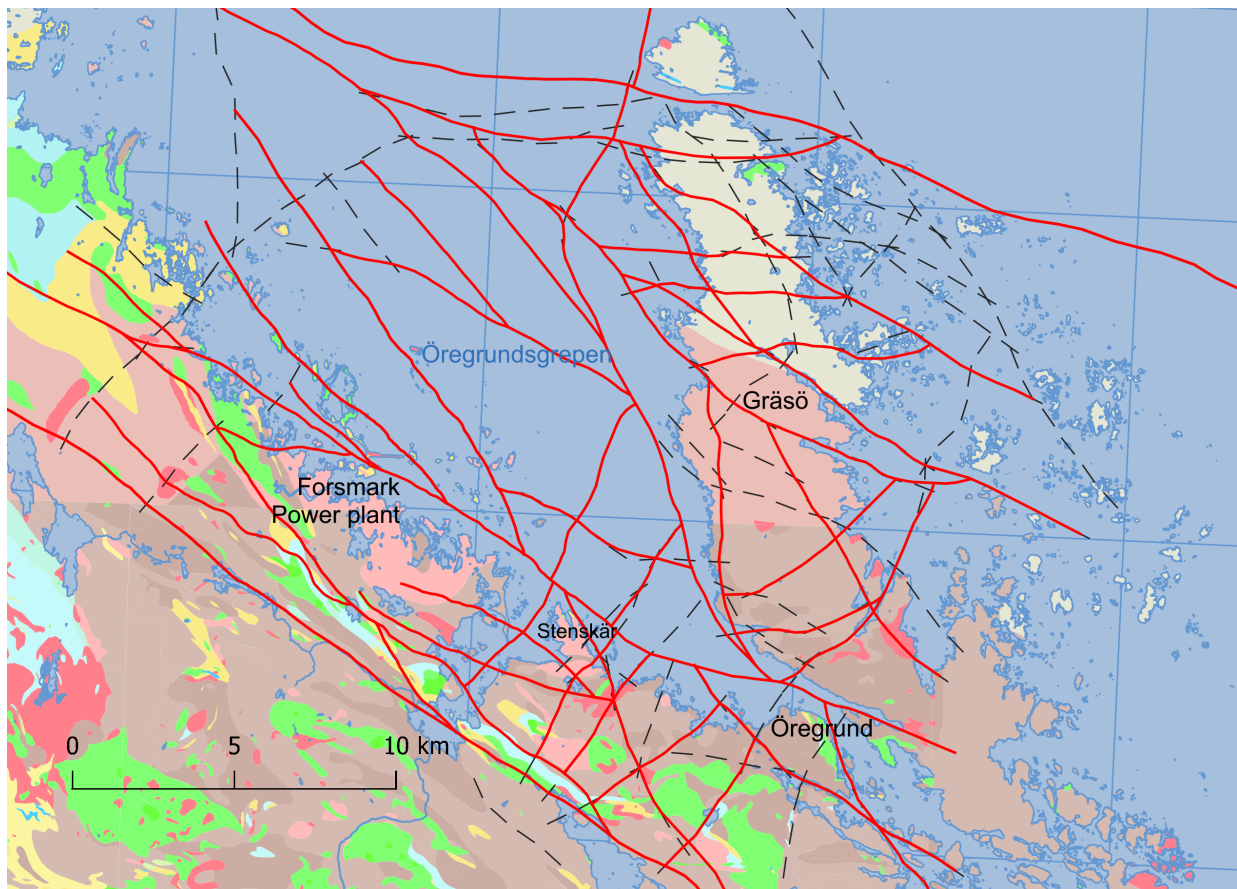


Fig. 3.2. Lineament model after Isaksson & Johansson (2020) subsequently used by Petersson & Hultgren (2021, in prep.) to model deformation zone trace lines, depicted by the red lines. Black dashed lines represent omitted lineaments from the model by Isaksson & Johansson (2020). Basemap: SGU bedrock map, originally scale 1:50000 (southern area) and scale 1:250000 (northern area).

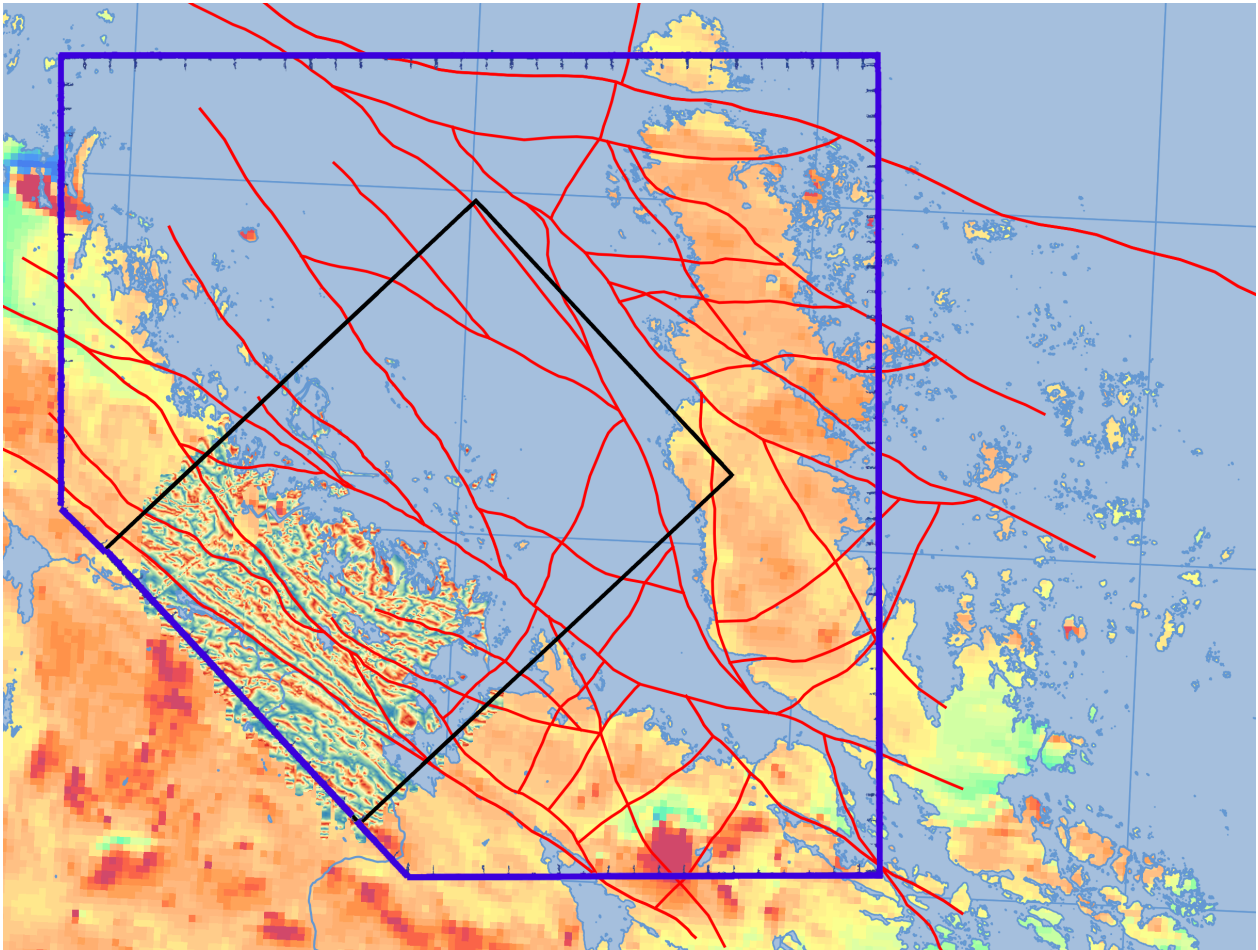


Fig. 3.3. SGU Magnetic field basemap used for the expanded work area (blue outline with perpendicular dashes) with superimposed magnetic field basemap in the regional model area (black rectangle). Red lines depict surface trachelines for modelled deformation zones by Hultgren & Petersson (SKB 2020), based on the lineament interpretations of Isaksson & Johansson (2020).

3.3 Stage 2 field data collection: detailed structural analysis

Stage 2 was undertaken with the aim to perform a detailed structural analysis on each deformation zone verified from stage 1, as well as a few new localities. The detailed structural analysis involved analysing shear sense indicators and relative age relations of fractures. Drone surveys of suitable outcrops were done using a DJI Phantom 4 with an RTK module in order to achieve an overview over the visited outcrops. Rendering of photo orthomosaics from the drone footage was done with the software Agisoft Metashape (version 1.7.2, 2021).

4 Results

This chapter focusses on field observations from both confirmed lineaments, where a deformation zone was observed in accordance with the location of the lineament, and new deformation zones that do not correspond to any previously inferred lineament. A summary of the results from the two field stages is presented in figure 4.1. In total, five lineaments have been verified as large-scale deformation zones in this project. Four of them are striking either NW-SE or NNW-SSE (Fig. 1; table 4.1). All five verified

lineaments include a mylonitic fabric, with four of them including a breccia as well (Fig 1; table 4.1).

Seven new deformation zones were discovered that do not correlate to any of the large-scale lineaments interpreted by Isaksson & Johansson (table 4.2). Five of them have a more or less 080-260 strike, are steeply dipping, and brittle in nature. They are found along the coast of southern Gräsö to central Gräsö, with one locality northwest of Öregrund. The NW-SE striking brittle zones are found close together near the bay of Norrhöljan and are thus referred to as the Norrhöljan bay zones in this chapter.

From a total of 52 visited localities (33 during stage 1 in late September – early October 2020 and 19 during stage 2 in late April 2021), a selection has been made to be included in this chapter. In early 2021, before stage 2 data collection of this project, Jesper Petersson (GEOS) visited three E-W trending lineaments in the north of Gräsö (ZFMEW3523, ZFMEW3513, ZFMEW3514) to verify the interpretations from stage 1 of this project.

Where applicable, the main results from the two field stages are presented in tables containing the following information for each deformation zone:

- Coordinates of the localities
- Trend of the deformation zone trace

- When measured, strike and dip following the right-hand-rule (RHR) method
 - Magnetic susceptibility
- These data are accompanied by a drone-photo orthomosaic or an orthophoto from Lantmäteriet as well as a schematic overview of the outcrop.

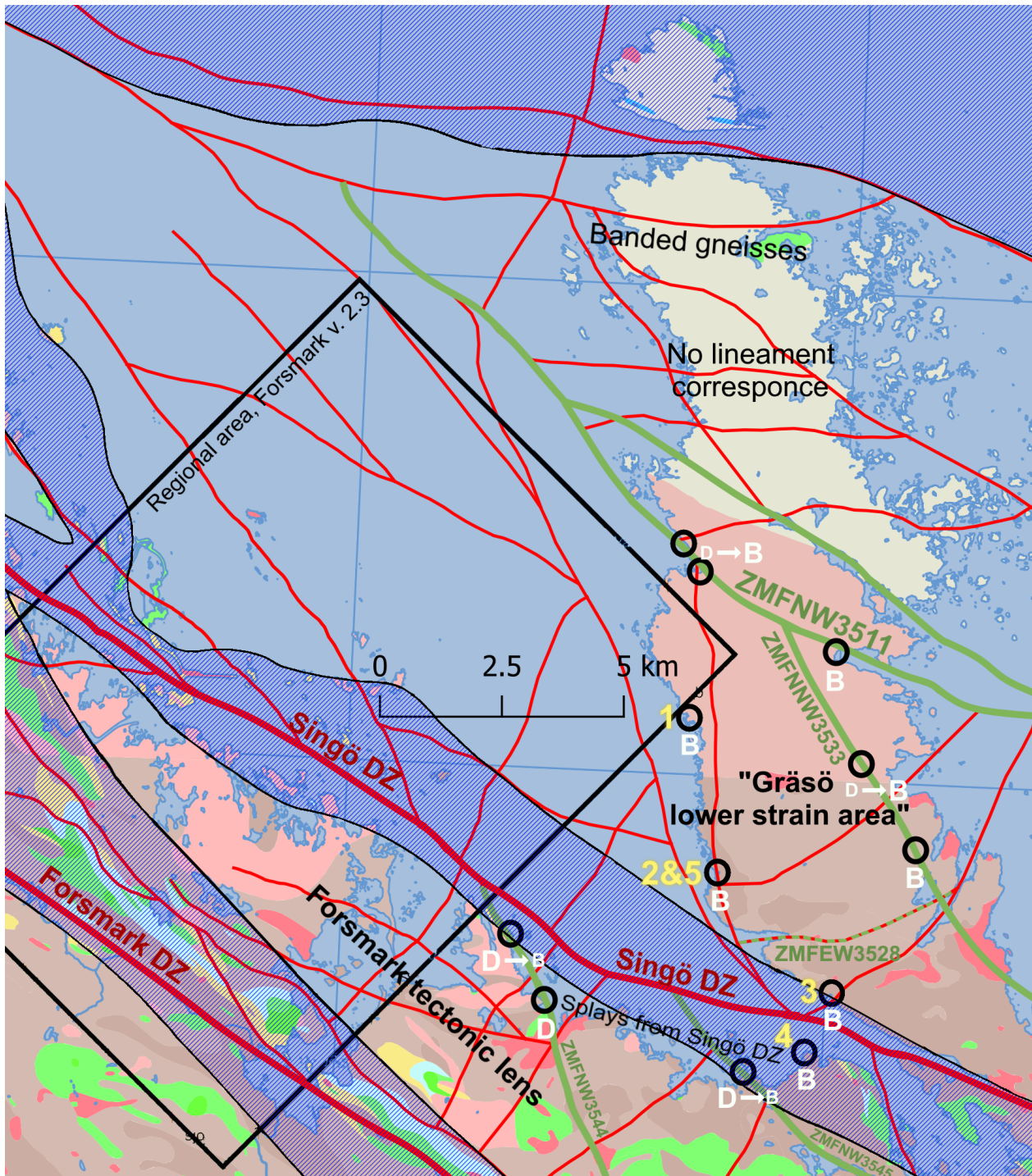


Fig. 4.1. Lineament investigation results on Gräsö and the southeastern area between the Singö DZ and the Forsmark DZ. Blue shaded areas: inferred to be affected by high ductile strain (Stephens et al. 2007). Green lineaments: Confirmed deformation zones. Black circles: Localities of found deformation zones. D & B markers stand for 'ductile' and 'brittle' respectively and indicate which type of deformation is visible at each locality. Basemap: SGU bedrock map, originally scale 1:50000 (south) and 1:250000 (north).

Deformation zone name: ZFM [trend] [4-letter no.]	Fault rocks	Width
ZFMNW3511	Mylonite and breccia	~400 metres
ZFMNNW3533	Mylonite and breccia	> 10 metres
ZFMEW3528*	Mylonite	Unspecified
ZFMNW3545	Mylonite and breccia	> 25 metres
ZFMNW3544	Mylonite and breccia	> 20 metres; < 40 metres

Table 4.1. Verified lineaments in this project. *Not completely E-W trending, more curved from E-W in the west of Gräsö to NW-SE to the east of Gräsö. NW-SE to the east of Gräsö.

Main stop corresponding to new deformation zone observation:	Trend	Width
ABR200016 ('1' on Fig. 4.1)	080-260 E-W	40 metres
ABR200014 ('2' on Fig. 4.1)	085-265 E-W	~10 metres
ABR210010 ('3' on Fig. 4.1)	080-260 E-W	> 15 metres
ABR200033 ('4' on Fig. 4.1)	075-255 E-W	10-15 metres
ABR200029	315-135 NW-SE	~0.45 metres
ABR210001 ('5' on Fig. 4.1)	330-150 NW-SE	~2 metres
ABR210016	330-150 NW-SE	~4 metres

Table 4.2. Newly discovered deformation zones in this project.

4.1 NW-SE, WNW-ESE and NNW-SSE deformation zones

Outcrop data from field observations for the NW-SE, WNW-ESE and NNW-SSE deformation zones described in this section are separated in two subsections, depending on to their location relative to areas inferred to be affected by higher and lower strain, as defined by Stephens et al. (2007) depicted in

figure 2.3. The deformation zones described in sub-section 4.1.1 are inside higher strain area, south of the Singö deformation zone. The deformation zones described in sub-section 4.1.2 are located north of the Singö deformation zone, inside of a tectonic lens.

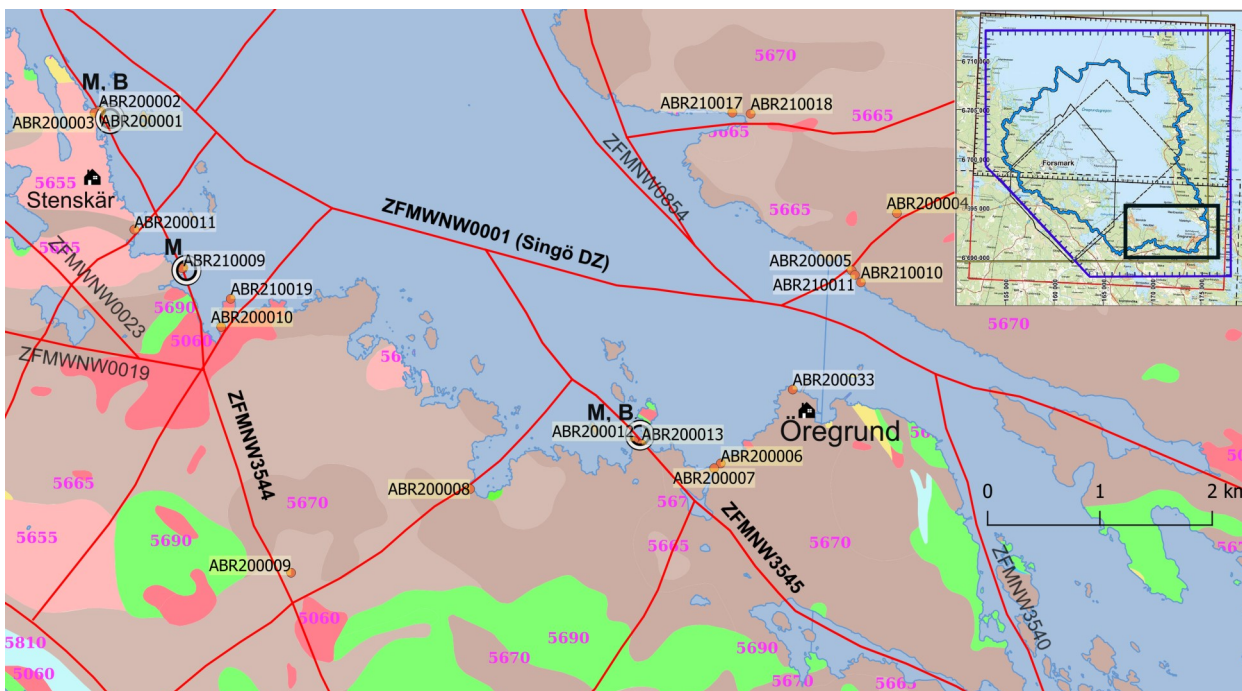


Fig. 4.2. Detail of the coast between Öregrund and Stenskar with only NW-SE and WNW-ESE lineaments marked. Circled areas with 'M' and 'B' labels are the corresponding field stops described in this section. 'M' and 'B' labels correspond to mylonite and breccia, respectively. Basemap: SGU bedrock map, originally scale 1:50000.

4.1.1 Coast between Öregrund and Stenskär

In the southeast corner of the expanded model area, there are several NW-SE and WNW-ESE trending lineaments (Fig. 4.2): ZFMNW3544, ZFMNW3545 and ZFMNW3540 originate from lineament ZFMWNW0001, which corresponds to the extensively studied Singö Deformation Zone. Lineament ZFMNW3544 has been observed in coastal outcrop ABR200001 and similarly striking mylonites have been observed in coastal outcrop ABR210009, further to the SE. Lineament ZFMNW3545 has been verified

in one coastal outcrop stop: ABR200012. Lineament ZFMNW3540 has not been observed. Lineament ZFMNW0854 is a high-confidence lineament which does not intersect with any land area and therefore could not be observed. The WNW-ESE trending lineaments ZFMWNW0023 and ZFMWNW0019 were originally modelled within the regional area and therefore not visited as part of this project.

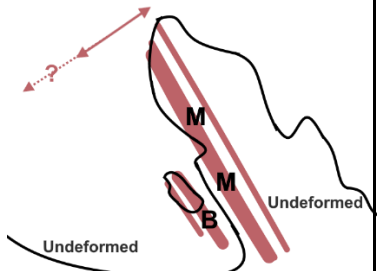
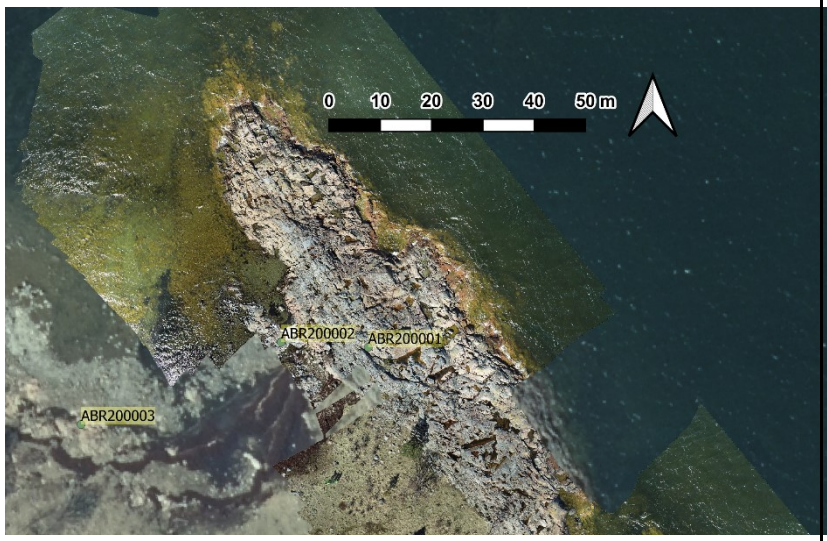


ZFMNW3544	
ABR200001	
Coordinates SWEREF99 18 00	6694698 N 0168032 E
Trend	330 - 150
Strike/dip Right hand rule	150/90
Magnetic susceptibility	$\sim 0,04 \cdot 10^{-3}$ (SI units)
	
	
ABR210009	
Coordinates SWEREF99 18 00	6693305 N 0168767 E
Trend	330 - 150 010 - 190
Strike/dip Right hand rule	150/90 190/90
Magnetic susceptibility	$\sim 0,4 \cdot 10^{-3}$ (SI units)
	
	

Table 4.3. Outcrop data of lineament ZFMNW3544, accompanied by orthophotos showing precise GPS locations as well as a schematic overview of each outcrop. The mylonites and local breccia are very well exposed.

At locality ABR200001, two ultramylonitic bands with parallel fracture zones are situated in a gneissic granitoid rock with subordinate mafic enclaves. The host rock has a vertically dipping gneissic foliation striking 150. The largest of the two mylonitic bands at ABR200001 has a thickness of 1,5 – 2 m (Fig. 4.3A). At location ABR200002 (6694699 N 0168015 E), a breccia with a minimum width of 3 m across strike contains ultramylonitic clasts and is located in a topographical low compared to the area containing the mylonites (Fig. 4.3B). The breccia is parallel to the ultramylonites and shows red-staining and is cemented by quartz veins. At ABR200003, around 40 m west of ABR200001, undeformed gneissic granitoid rocks crop out. This is thus the maximum possible extent of the deformation zone.

At locality ABR210009, several parallel NW-SE striking mylonites are situated in a granitoid rock with

subordinate mafic enclaves. The host rock has a ductile fabric with a tectonic foliation with an orientation of 060/40. About 10 m to the west two vertical fractures with mylonites occur striking 190. From these mylonites splay several smaller mylonites with a more NE-SW strike (Fig. 4.4). On this outcrop, a kinematics study has been performed on the visible subhorizontal plane, with further details in chapter 5.



Fig. 4.3. **A.** ABR200001: Vertically dipping ultramylonite striking 150, parallel to lineament ZFMNW3544. View on the photo is along its strike. **B.** ABR200002: Breccia (under water) parallel to the mylonite in Fig. 4.3. View on the photo is along its strike.



Fig. 4.4. ABR210009: Vertically dipping mylonitic bands striking 150 (dark-coloured bands in middle of photo).

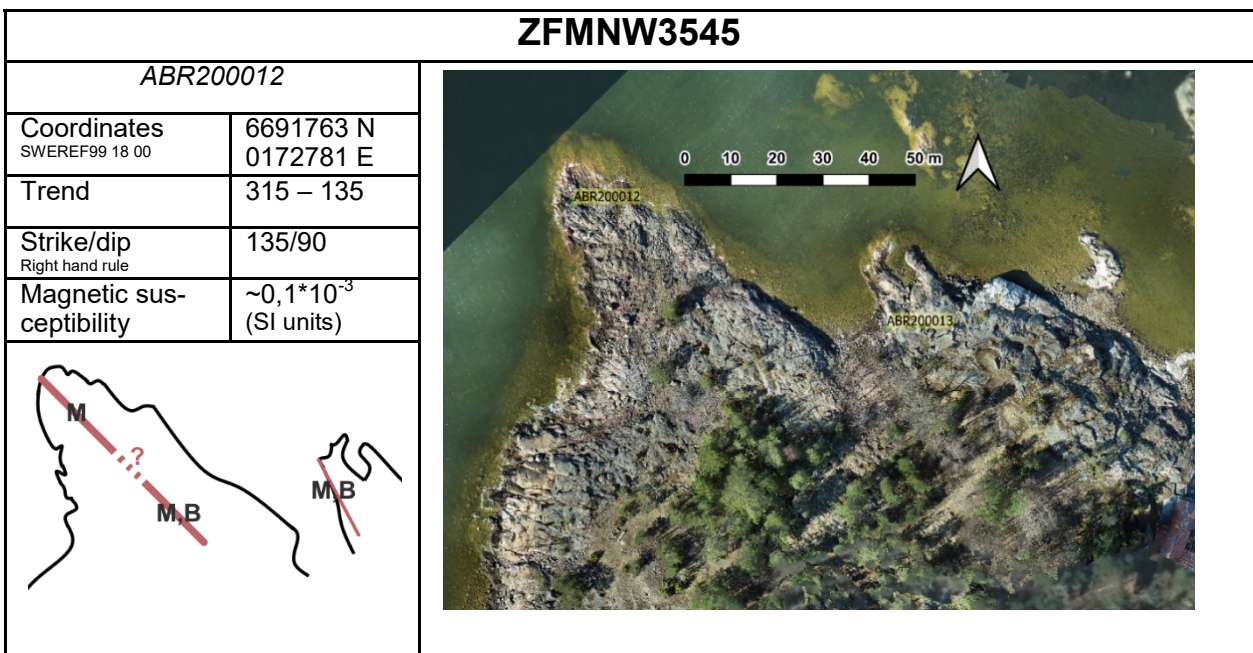


Table 4.4. Primary outcrop data of lineament ZFMNW3545, accompanied by an orthophoto showing precise GPS locations of localities as well as a schematic overview of the outcrop. The two mylonite and breccia localities are well exposed.

At locality ABR200012, a c. 1 m wide vertically dipping mylonite striking 135 runs from the tip of the outcrop (at ABR200012) until it is covered by vegetation. Locally inside the mylonite, breccias about 5 cm wide run with the same strike (Fig. 4.5). At ABR200013 (6691736 N, 0172849 E), a second mylonite and breccia striking 150 runs at the side of the rock. This second zone is not as wide and hosts more breccias than the main mylonite. The surrounding host rocks are made up of a medium- to fine grained metagranitic rock with no apparent

foliation. Its magnetic susceptibility is about $7 \cdot 10^{-3}$ (SI units).



Fig. 4.5. ABR200012: Breccia associated with mylonite. Breccia clasts are in part made up of mylonitic rocks.

4.1.2 Central Gräsö

In the middle of Gräsö, there are two NW-SE trending lineaments (ZFMNW3519 and ZFMNW3511), both clearly visible on magnetic, VLF, and topographical maps. In between these lineaments, SGU's bedrock maps place the contact between gneissic granitoids in

the south and gneisses in the north (Fig. 4.6) Lineament ZFMNNW3533 is inferred to terminate against the NW-SE trending lineament ZFMNW3511 (Fig. 4.5). Both ZFMNW3519 and ZFMNW3511 are classified as high-confidence lineaments, however, no outcrops were found for the high-confidence level lineament ZFMNW3519.

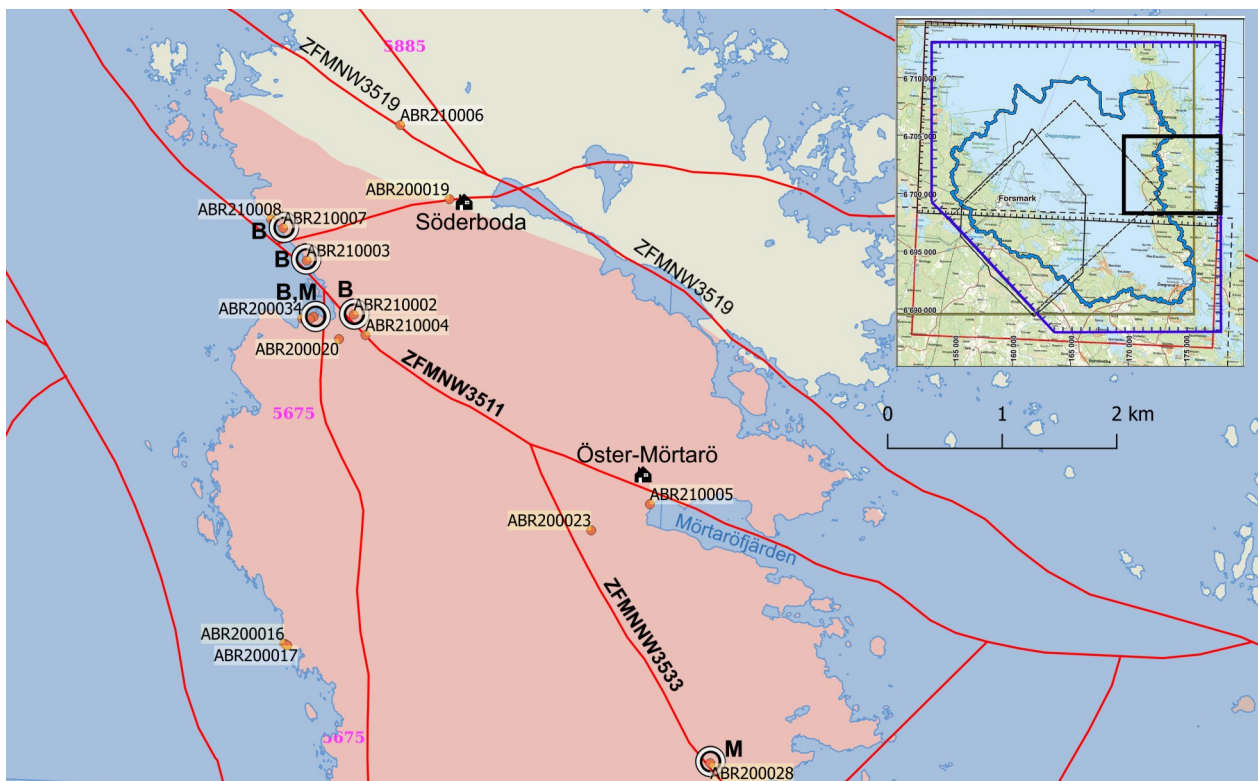


Fig. 4.5. Detail of central Gräsö with the townships Söderboda and Öster-Mörtarö. Only the NW-SE and WNW-ESE lineaments are marked. Circled areas with labels are the corresponding localities described in this section. 'M' and 'B' labels correspond to mylonite and breccia, respectively. Basemap: SGU bedrock map, originally scale 1:250000.



Fig. 4.6. Orthophoto overview of the localities of NW-SE striking brittle zones at the coast of Norrhöljan bay (from north to south: ABR200029, ABR210001 and ABR210016) and their location relative to nearby Djursten.

Lineament ZFMNW3511 is characterized by strongly red-stained breccias, with distinctive vuggy veins between clasts. The rocks surrounding the breccias show a high fracture density and are red-stained as well. Exposure along the west coast of Gräsö is good, and the breccia could be observed in several outcrops along the coast (Figs. 4.8 and 4.9). However, further inland and on the east coast, following the lineament, the bedrock is mostly covered by agricultural fields. Only at the side of the road to Öster-Mörtarö and near the shore of Mörtaröfjärden (Fig. 4.5), some small outcrops are found showing red-stained rocks and vuggy quartz veins (ABR210004, Fig. 4.10A and ABR210005, Fig. 4.10B).

Multiple sets of NW-SE striking zones (ABR200029, ABR210001, ABR210016) are found at the 'Norrhöljan' bay, about 500 metres north of the township Djursten (Fig. 4.7). They are brittle fracture zones characterised by an increased fracture frequency through metagranitic rock. The fractures are filled with fine-grained adularia and laumontite as well as larger aggregates of fractured calcite. The NW-SE zone at locality ABR210016 is cross-cut by a 010-190 striking fracture.

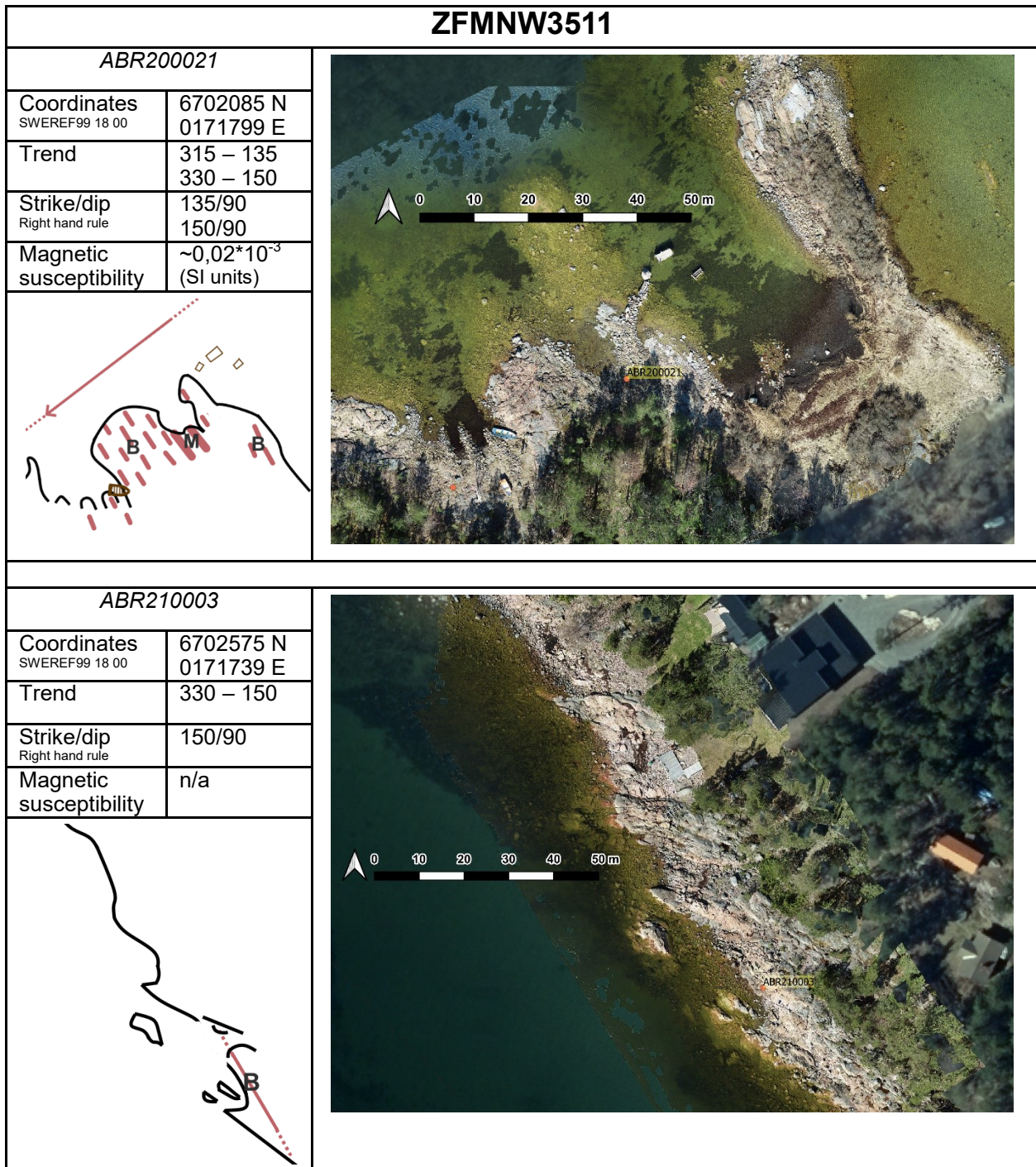


Table 4.5. Outcrop data of lineament ZFMNW3511, accompanied by orthophotos showing precise GPS locations of localities as well as a schematic overview of each outcrop. There is a good exposure of the highly fractured, red-stained rocks.

The collection of localities on figure 4.5 covered by stop label 'ABR200034', feature an intensely fractured and completely red-stained breccia, with abundant quartz veins striking between 135 and 150 (Fig. 4.8A). In the schematic overview in Table 4.5, the extent of this breccia on the outcrop is depicted as short red dashes. In the bay inlet at ABR200021, a glassy banded rock is visible in a topographical low close to the water's edge (Fig. 4.8B).

At locality ABR210003, a 0.5 m wide fracture set with vertically striking fractures striking 150 occurs (Fig. 4.9A). One contains a brecciated vein in the

middle (Fig. 4.9B). The fractures have the same strike as the breccia vein at the roadside outcrop ABR210002 (Fig. 4.6). Following the rocky shore to the northwest, more fracture sets are found (ABR210007, breccia striking 340 and ABR210008, fracture group striking 315).



Fig. 4.6. A. Overview of outcrop within ZFMNW3511 facing the north. Picture taken standing on heavily fractured and intensely red-stained outcrop. Small bay inlet corresponding to stop ABR200021 is seen on the right-hand side where the shade of the tree falls. On the other side of the water at the tree line is outcrop ABR210003. **B.** ABR200021: Banded mylonite within ZFMNW3511.



Fig. 4.9. **A.** ABR210003: Top-down view of a band showing grain size reduction (mylonitisation) cut by the 0.5 meter-wide fracture set. **B.** ABR210003: Vertically dipping sealed fracture network striking 150.



Fig. 4.10. **A.** ABR210004 (6701923 N, 0172252 E) and **B.** ABR210005 (6700446 N, 0174736 E): Characteristic vuggy veins and brecciated red-stained rock corresponding to lineament ZFMNW3511. The vuggy quartz vein in ABR210005 strikes 300.

ZFMNW3533

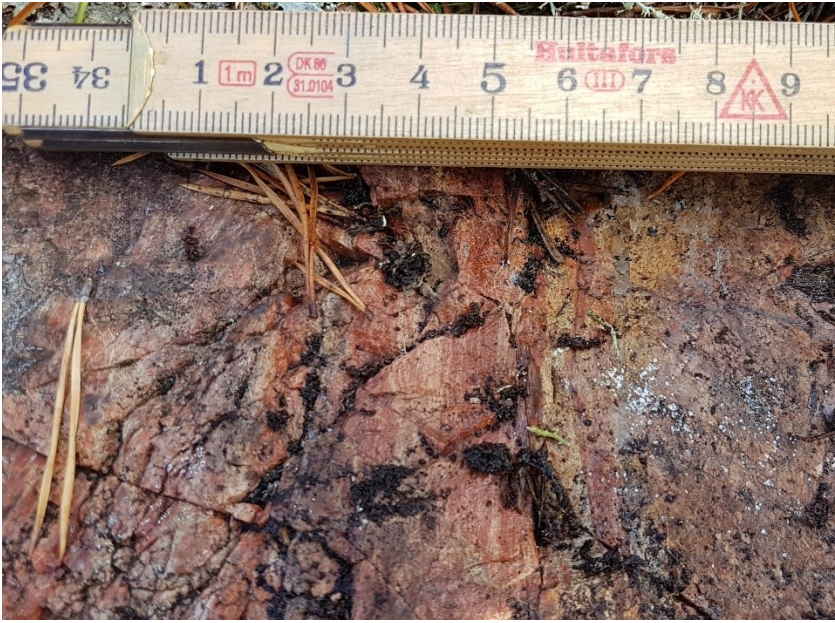
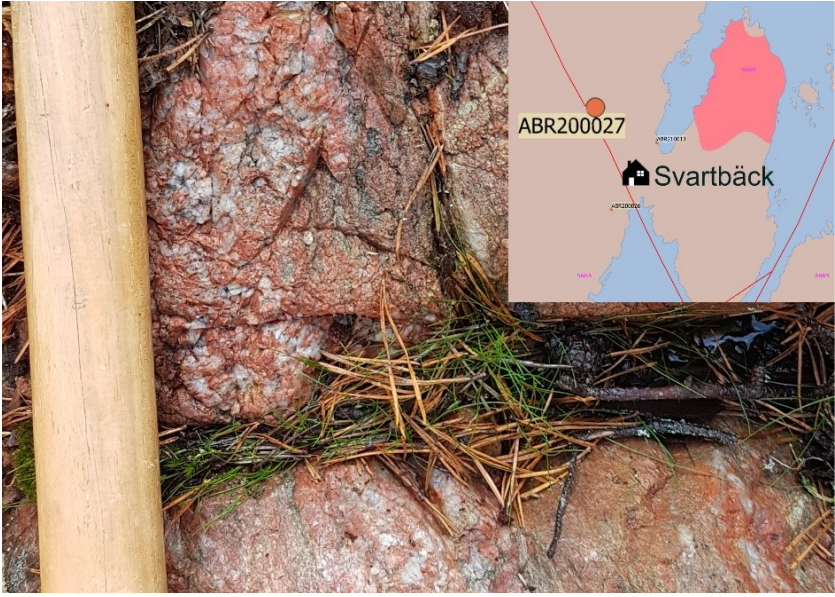
ABR200028		
Coordinates <small>SWEREF99 18 00</small>	6698183 N 0175264 E	
Trend	330 – 150	
Strike/dip <small>Right hand rule</small>	150/90	
Magnetic susceptibility	n/a	
ABR200027		
Coordinates <small>SWEREF99 18 00</small>	6696373 N 0176398 E	
Trend	340 – 160 350 – 170	
Strike/dip <small>Right hand rule</small>	160/? 170/?	
Magnetic susceptibility	$\sim 0,2 \cdot 10^{-3}$ (SI units)	

Table 4.6. Primary outcrop data of lineament ZFMNW3533, accompanied by field photos. The banded rock at ABR200028 follows the same lineament as the breccia at ABR200027.

At locality ABR200028, there is a small (± 7 cm wide) vertically dipping mylonite, striking 150, in a moss-covered outcrop at the edge of a forest. The host rock is a coarse-grained red-coloured granitic rock.

At locality ABR200027, there is a ± 10 meter wide highly fractured granitic rock located at the side of the road from Svartbäck to Kallvik. On the outcrop, which is a topographical high compared to the road, some parts are more brecciated than others. The most brecciated part is situated roughly in the middle (illustrated here). All breccias strike between 340 and 350. The host rock is a fine-medium grained granitic rock with a high frequency of pegmatitic veins.

NORRHÖLJAN BAY ZONES


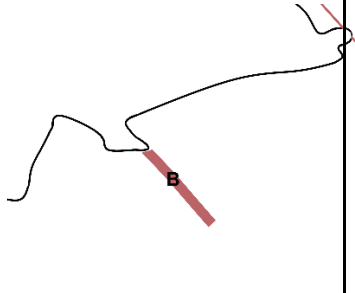



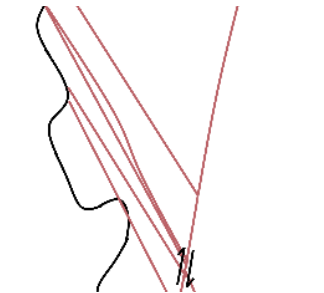
<i>ABR200029</i>		
Coordinates <small>SWEREF99 18 00</small>	6695889 N 0172341 E	
Trend	315 – 135	
Strike/dip <small>Right hand rule</small>	135/90	
Magnetic susceptibility	n/a	
		
<i>ABR210001</i>		
Coordinates <small>SWEREF99 18 00</small>	6695822 N 0172282 E	
Trend	330 – 150	
Strike/dip <small>Right hand rule</small>	150/90	
Magnetic susceptibility	n/a	
		
<i>ABR210016</i>		
Coordinates <small>SWEREF99 18 00</small>	6695701 N 0172283 E	
Trend	330 – 150 010 – 190	
Strike/dip <small>Right hand rule</small>	150/90 190/90	
Magnetic susceptibility	n/a	
		

Table 4.7. Primary outcrop data of the Norrhöljan bay zones accompanied by orthophotos showing precise GPS locations of localities as well as a schematic overview of each outcrop. 28

The protruding ridges in the southwest of Gräsö, near the bay called 'Norrhöljan' (Fig. 4.7), expose a variety of brittle fracture sets (Fig. 4.11). At the northern end, a couple of parallel 080-260 striking brittle zones (set C), that vary in thickness with its widest zones in the south end from ~0,5 m (most prominent ones, ABR200014 and ABR200015) to ~0,2 m, with four smaller parallel sets to the north. These 080-260 striking zones are steeply dipping and discrete and envelop rock lenses in the middle unaffected by brittle deformation. A more shallowly dipping chlorite-filled

fracture is crosscut by one of these zones. Slickensides plunging 35° towards 045 are visible on the crosscut 355/40 fracture plane. Roughly parallel to the NW-SE trending outcrop ridges are the brittle zones attributed to set B. These zones have the same fracture minerals to the set C zones and are also very steeply dipping. The intersection points of the widest zones from sets B and C would be beneath sea-level in the bay and are therefore not directly visible in the field.

At locality ABR200029, a 315-135 striking brittle zone creates bands of lower elevation in the outcrop

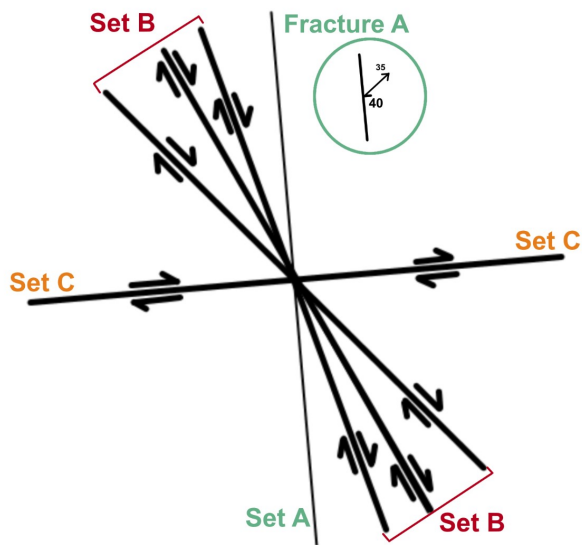


Fig. 4.11. Brittle deformation zones at localities (from N to S) ABR200014, ABR200015, ABR200029 & ABR210001. Kinematics interpreted from slickensides.

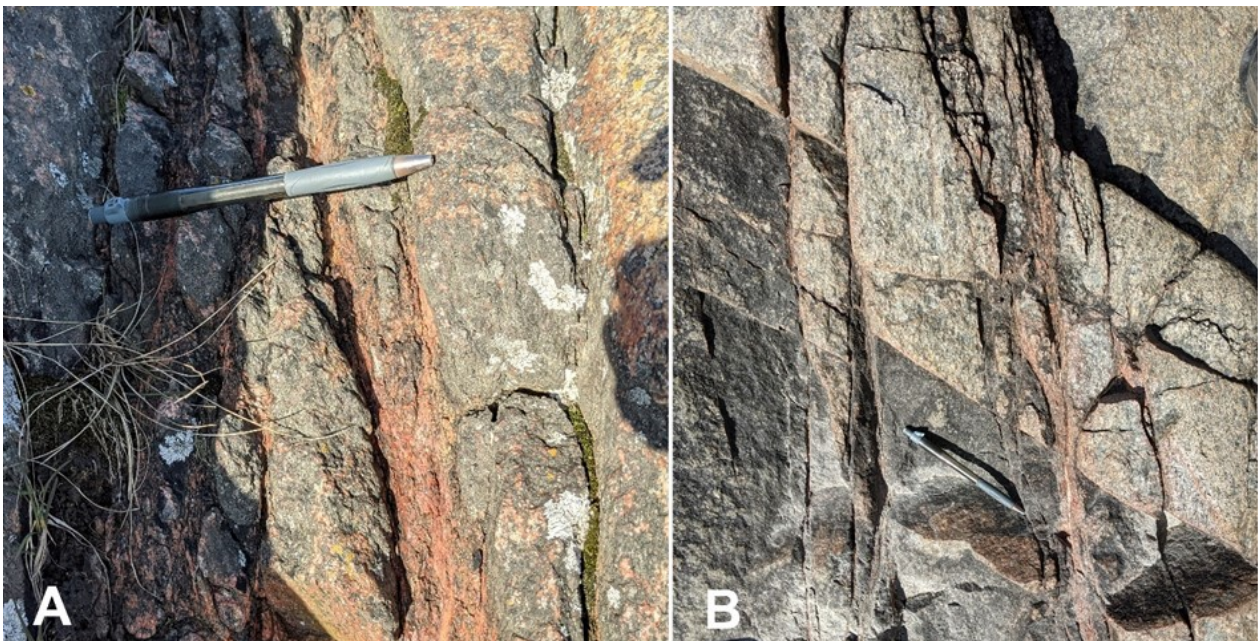


Fig. 4.12. ABR200029: A. Red-stained parallel fractures filled with fine-grained minerals making up one fracture zone. B. A parallel fracture zone horizontally displacing two host rock types.

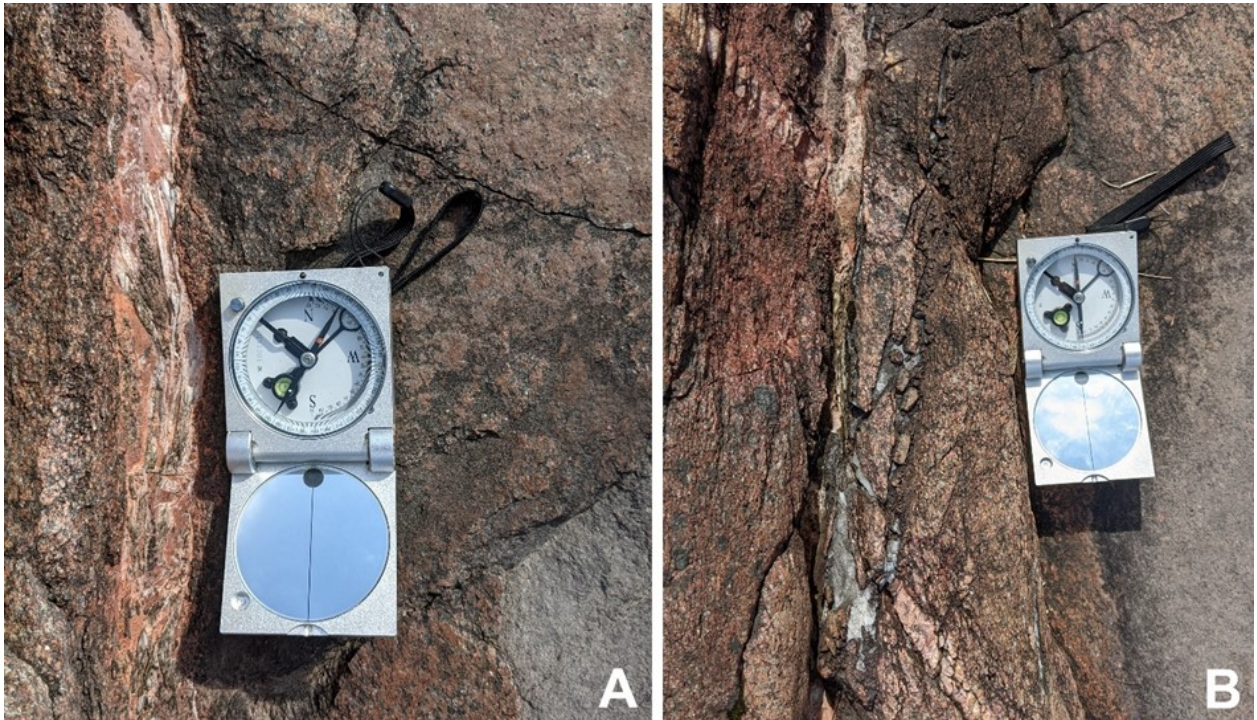


Fig. 4.13. ABR210016: **A.** A 330-150 striking fracture zone containing adularia and laumontite as well as calcite. **B.** 010-190 striking fracture zone dextrally displacing a felsic vein.

(Fig. 4.12A, B). Its fracture sets contain fine-grained adularia and laumontite as well as calcite.

Further south at ABR210001, a 330-150 striking zone cuts through a ridge in the same strike. One fracture plane reveals horizontal slickensides.

The southernmost locality of ABR210016 hosts a brittle zone containing multiple parallel fracture sets filled with fine-grained adularia and laumontite as well as calcite (Fig. 4.13A). They are horizontally offset by a 010-190 striking brittle fracture zone containing the same fracture mineral assemblage (Fig. 4.12B). About 120 m south of ABR210001 is locality ABR210016

(6695701 N, 0172283 E), which hosts a 3-5 m wide NW-SE trending brittle fracture zone, which is dextrally displaced by a roughly N-S trending smaller brittle zone (Fig. 4.14). Both zones have calcite and hematite-stained laumontite and adularia as fracture minerals.

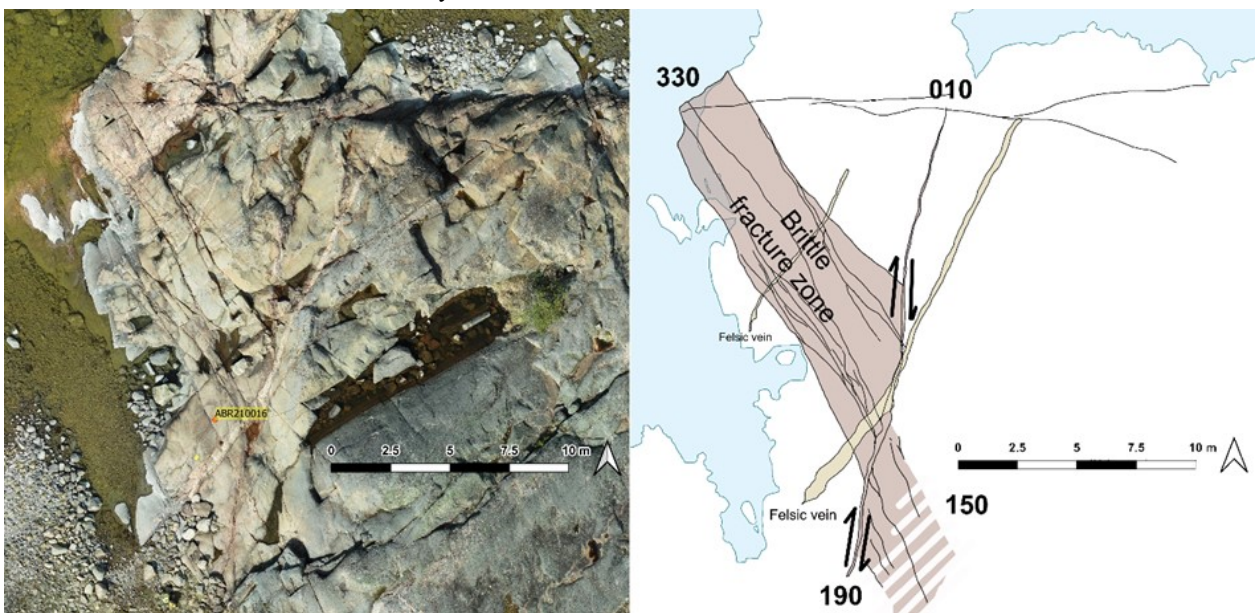


Fig. 4.14. ABR210016: Dextral displacement of a 330-150 trending brittle zone by a 010-190 trending brittle zone. Red halo around fractures is visible for both zones.

4.2 E-W (080-260 striking) deformation zones

In this sub-section, there are three approximately E-W striking zones observed, corresponding to outcrop numbers (from south to north) ABR200033, ABR210010, ABR200014 and ABR200017 (Fig.

4.15).

The four new zones described below do not show up on the magnetic or VLF geophysical maps, but they are visible in digital elevation maps on the places where they are also observed on outcrops. Any lateral continuation is not visible on any maps.

In appearance, these zones are very similar to each

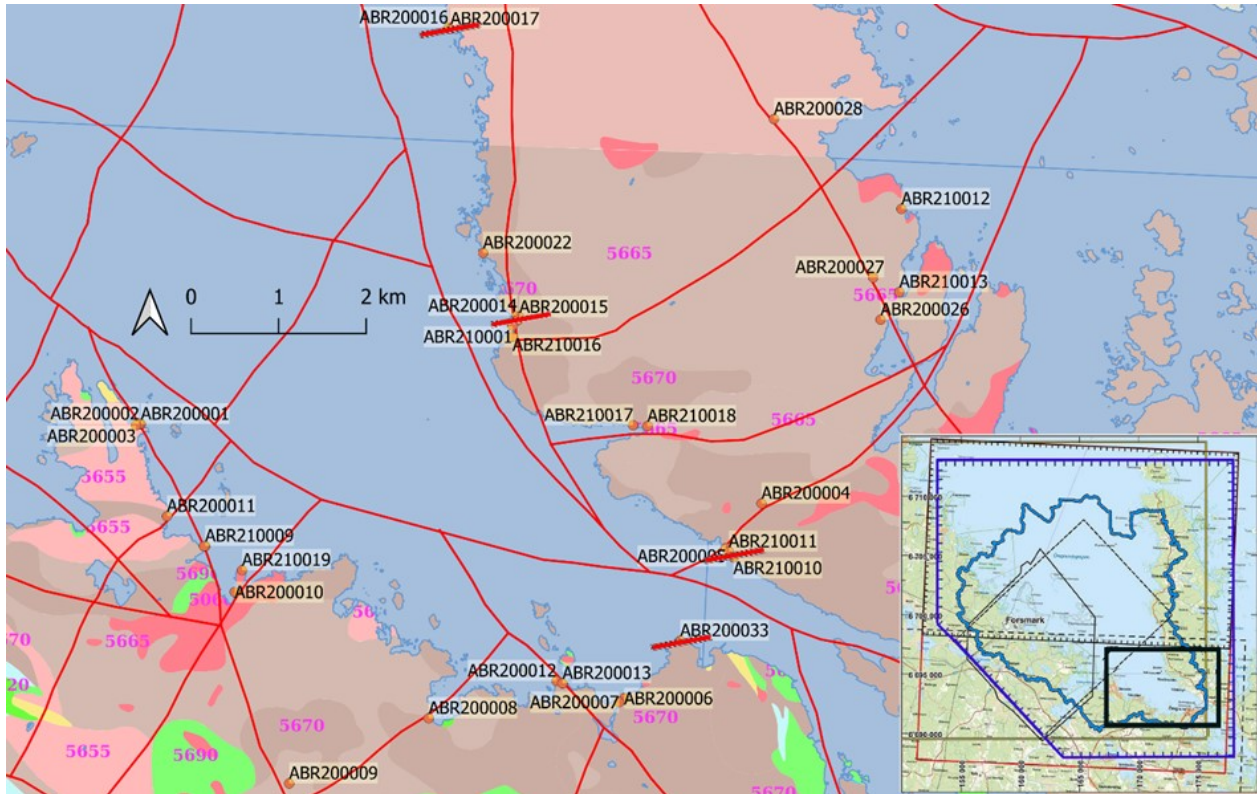


Fig. 4.15. 080-260 striking zones in Southern Gräsö and Öregrund. Trends are depicted by short red lines. The length of these lines in the figure is arbitrarily chosen and does not represent the observed length in the field. Basemap: SGU bedrock map, originally scale 1:50000 and originally scale 1:250000 (northern part).

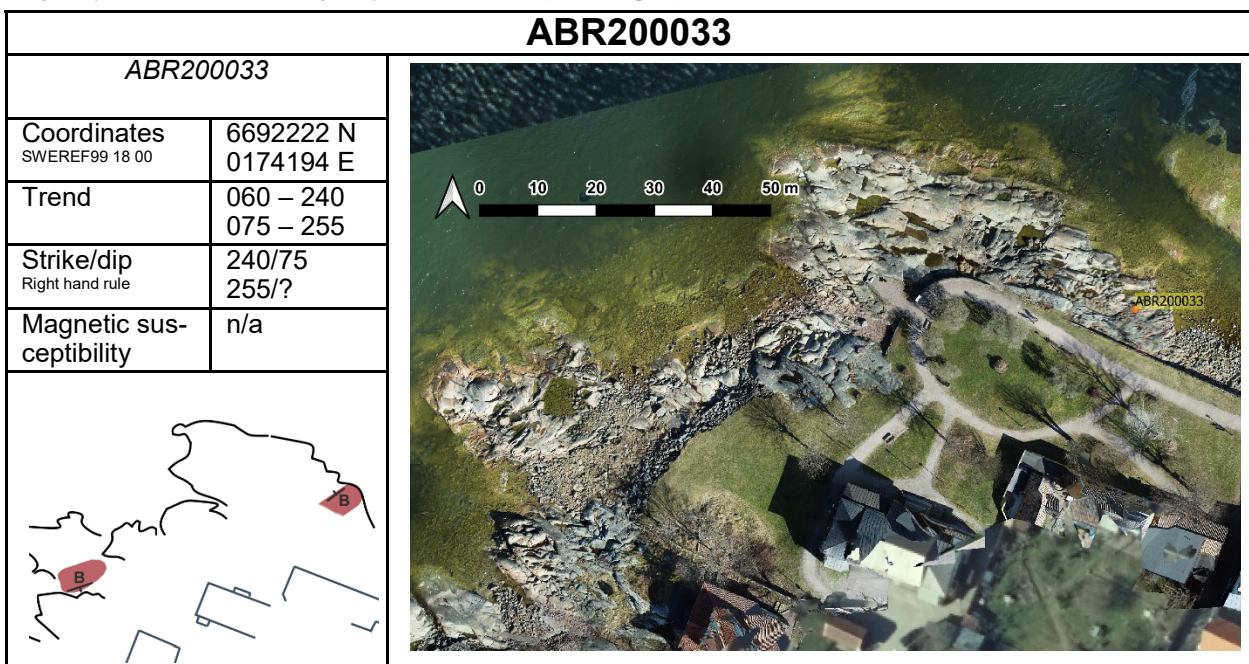


Table 4.8. Primary outcrop data of new deformation zone at locality ABR200033, accompanied by an orthophoto showing precise GPS locations of the locality as well as a schematic overview of the outcrop. There are two sections of brittle fracture zones at either end of the man-made infrastructure part of Öregrund.

other: brittle to semi-brittle, thoroughly red-stained zones with a high fracture frequency and fractures that meander somewhat around more or less undeformed lenses of the host rock. They are also observed to cross-cut the tectonic foliation.

The observed length of each of the three zones is unclear and solely dependent on the extent of each individual outcrop. The width of the zones is defined as the distance between the first appearance of thin bands of crushed rock to the last. Usually, there is no real core where the brittle to semi-brittle deformation is observed to be the most intense. The anastomosing bands can vary in thickness within each zone from

centimetre to decimetre scale.

At the north-western tip of Öregrund, there are two red-stained fracture zones striking approximately to WNW which cross-cut the foliation of the host rock. The first is located at ABR200033, where it runs from the sea to about 10 meters inland where it seems to disappear (Fig. 4.16A, B). This zone is 10 metres wide. At the other side of the tip, along the strike of the first fracture zone, a second fracture zone is visible with the same fine-grained red-stained fractures. This zone strikes slightly more E-W and is slightly wider.

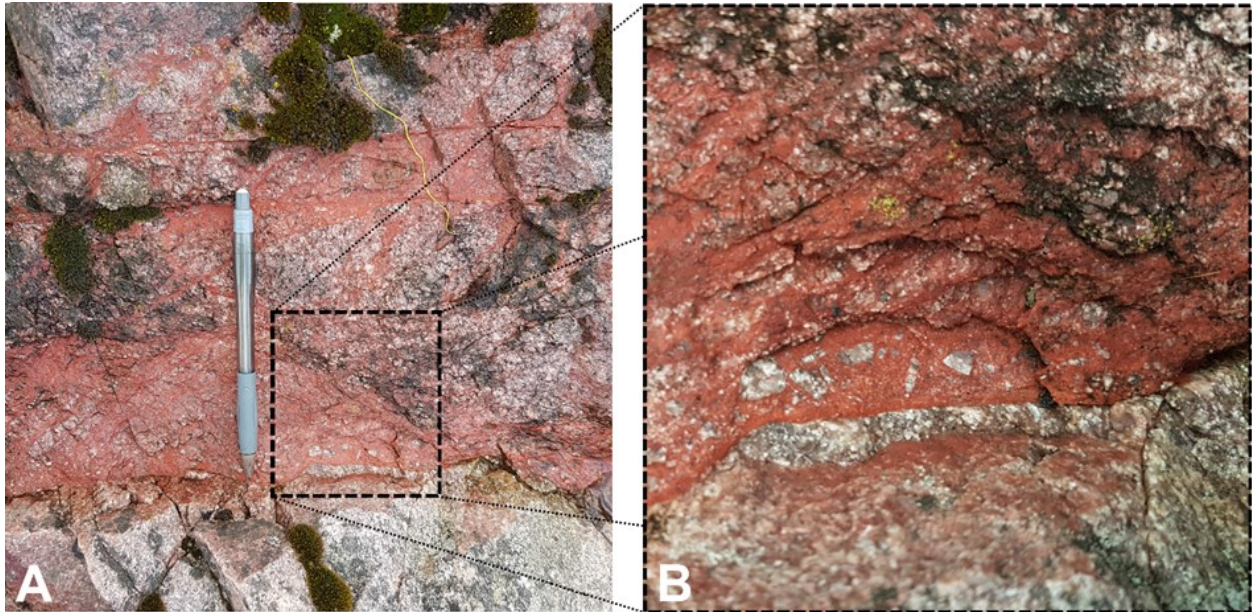


Fig. 4.16. A. ABR200033: Red-stained brittle fracture network, steeply dipping to the north. B. Detail of brecciated rock within the fracture network.

ABR210010	
<i>ABR210010</i>	
Coordinates <small>SWEREF99 18 00</small>	6693175 N 0174801 E
Trend	080 – 260
Strike/dip <small>Right hand rule</small>	260/70
Magnetic susceptibility	$\sim 0,15 \cdot 10^{-3}$ (SI units)

Table 4.9. Primary outcrop data of a new deformation zone at locality ABR210010, accompanied by an orthophoto showing precise GPS locations as well as a schematic overview of the outcrop. The outcrop in the southeast hosts the two brittle zones.

At the outcrops near the beaches of the Gräsöbadens Familjecamping, there are two parallel red-stained brittle fracture zones at ABR210010, dipping steeply to the north (Fig. 4.17). The two fracture zones are 1 and 1.5 metres wide, respectively. At ABR210011, a \pm 0.75-centimeter-wide fracture set with 8-10 red-

stained fractures subvertically dips to the east. Strike / dip (with right-hand rule) of ABR210011 is 035/85. The host rock at these outcrops is an L-tectonite with a mineral stretching lineation plunging 50 degrees towards 155.



Fig. 4.17. ABR210010: E-W striking steeply dipping red-stained fractures. The fracture minerals have a greatly reduced grain size compared to the crystalline host rock.

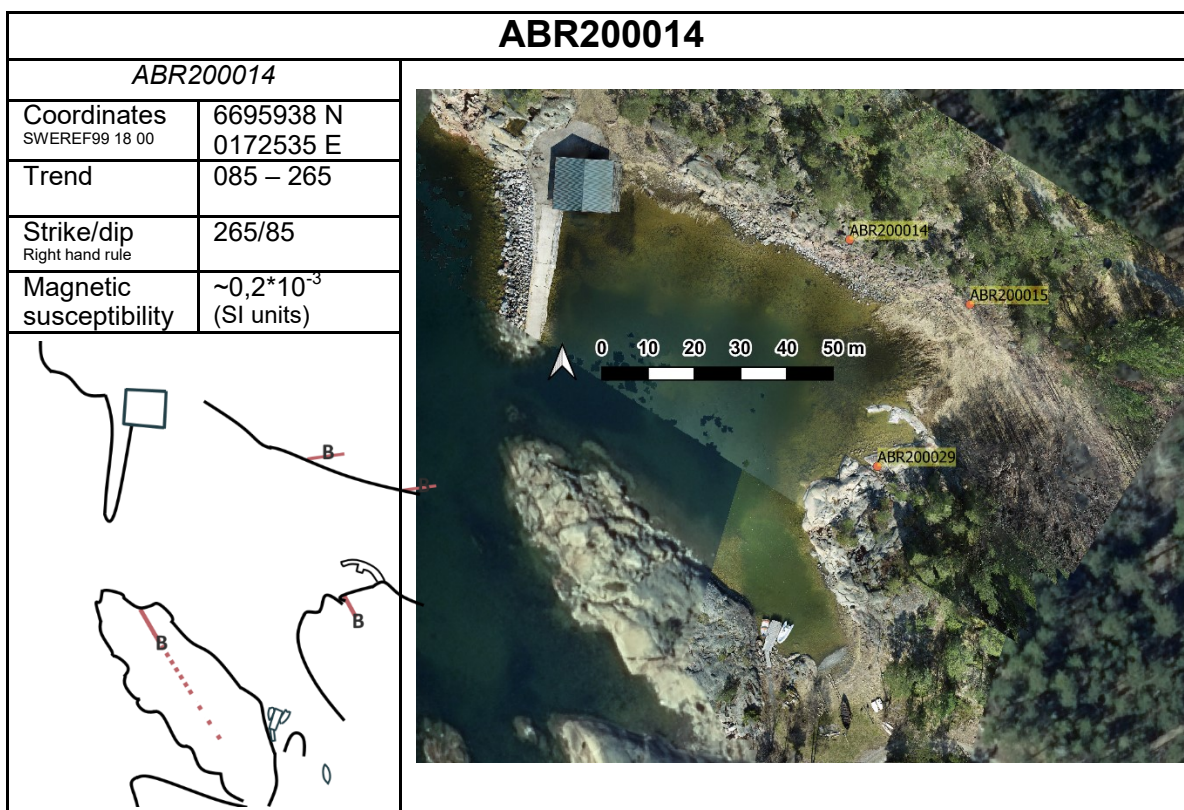


Table 4.10. Primary outcrop data of new deformation zone at locality ABR200014, accompanied by an orthophoto showing precise GPS locations of the localities as well as a schematic overview of the outcrop. There are several brittle zones around the small bay.

At the Norrhöljan bay inlets on the western shore of Gräsö, several E-W striking fracture zones can be distinguished: a 0.5 m-wide brittle, fine-grained, red-stained fracture zone (Fig. 4.18A), with 5 less wide fracture zones of the same nature parallel to it. These are locally cross-cut by 150-330 striking mineral-filled fractures.

In the area of central Gräsö, one more approximately E-W striking zone on the western shore was discovered (ABR200017, Fig. 4.19). This deformation zone is the clearest and largest example of a typical 080-260 striking zone, at a total of 40 metres wide from the first appearance of grain size reduction of fracture minerals to the last. ABR200017 would be

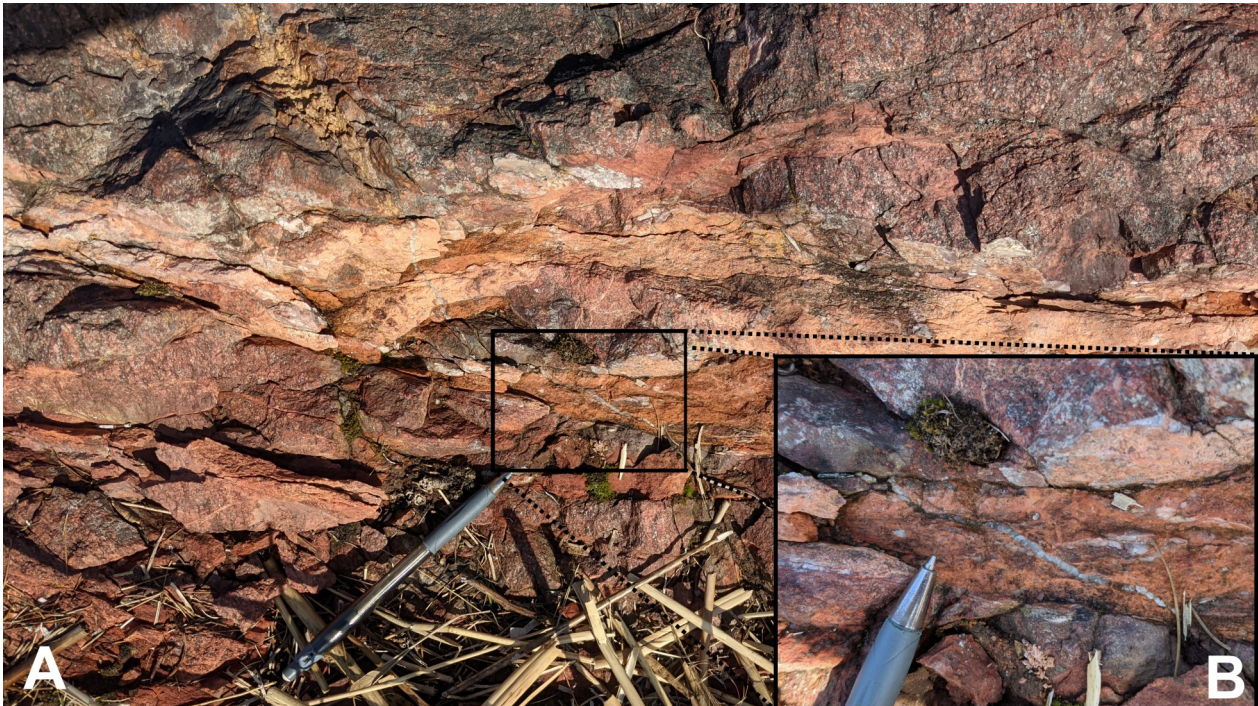


Fig. 4.18. ABR200014: A. Main 265-085 striking fracture zone (seen here roughly E-W, true north does not equal north of this picture). B. A ~0.5 cm wide mineral-filled 150-330 degrees striking fracture.

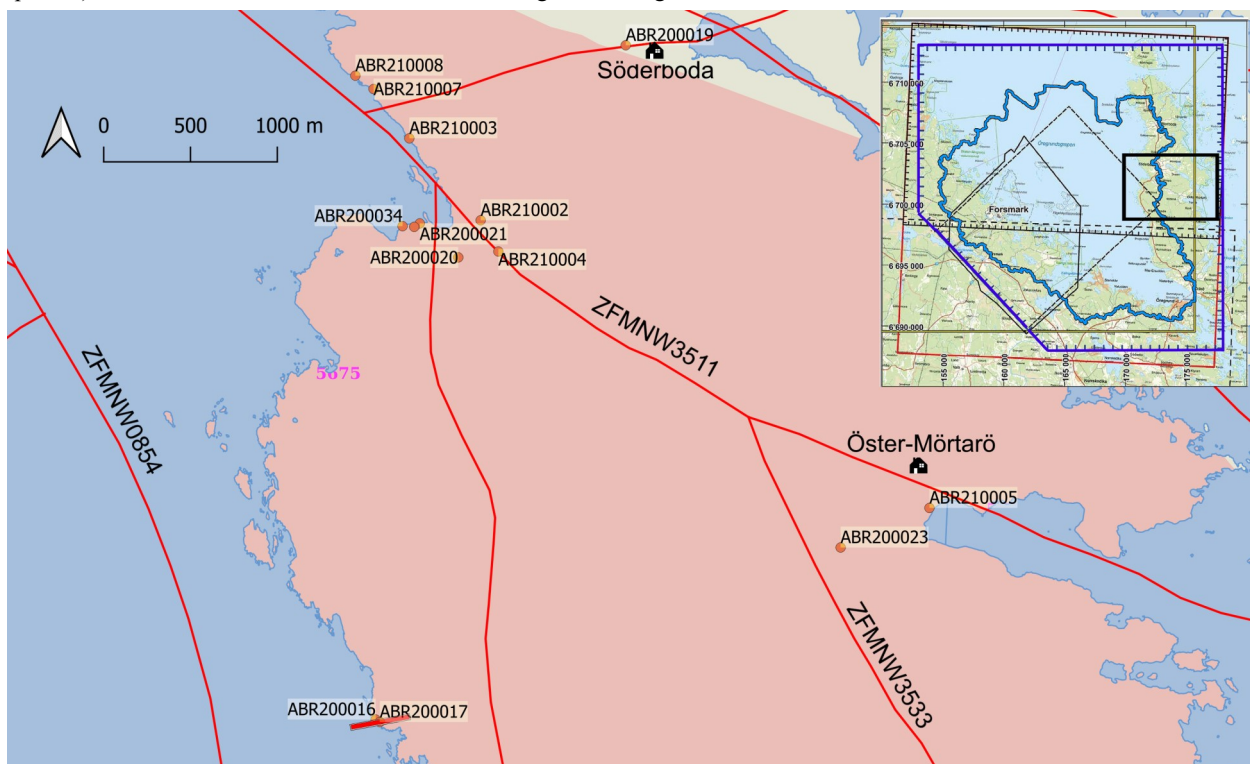


Fig. 4.19. Locality of ABR200017 in relation to the NW-SE striking lineaments ZFMNW0854, ZFMNW3511 and ZFMNW3533 in central Gräsö. Trend depicted by a short red line. The length of the line in the figure is arbitrarily chosen and does not represent the observed length in the field. Basemap: SGU bedrock map, originally scale 1:250000.

the ‘type locality’ of this type of deformation zone on Gräsö. It shares its appearance with the three southern zones described before, with strong red-staining,

brittle deformation and a great grain-size reduction compared to the host rock.

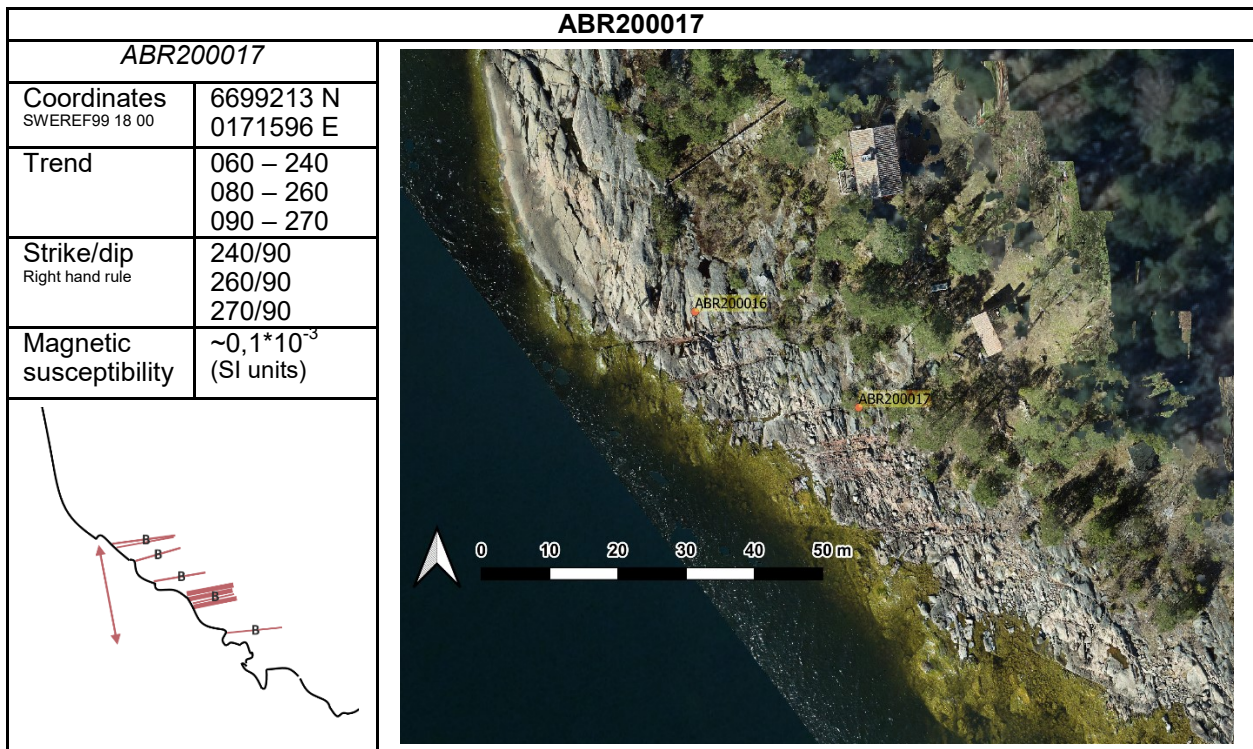


Table 4.11. Primary outcrop data of new deformation zone at locality ABR200014, accompanied by an orthophoto showing precise GPS locations of the localities as well as a schematic overview of the outcrop. There are several parallel brittle zones visible at their full width.



Fig. 4.20. ABR200017: Widest section of the deformation zone, where several parallel bands of very fine-grained fractures cut the host rock foliation at an almost 90-degree angle. Yellow field book (A5 size) for scale.

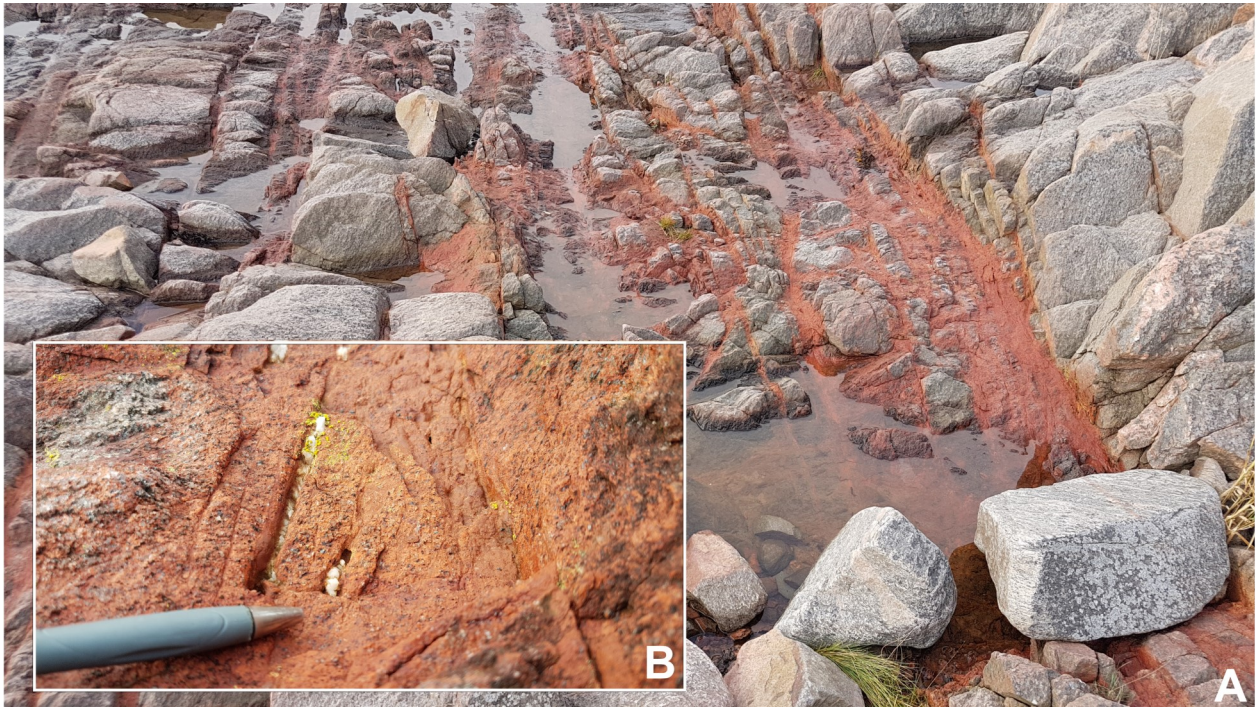


Fig. 4.21. A. ABR200017: View along the deformation zone and B. Close-up of the fracture (bottom left). The fine-grained fractures are clearly deeper eroded than the undeformed host rock.

At the south end of the central Gräsö, a curved topographic low is seen trending from E-W west of Gräsö to NNE-SSW in the east (Fig. 4.22A). On the SGU bedrock map by Stålhös (1989), this low is marked with several mylonite symbols, following the shoreline in the eastern section and intersecting with locality ABR210012 (6696156 N, 0176721 E) (Fig. 4.22B). The interpreted lineament ZFMEW3528 used for this study does not curve upward but instead terminates against lineament ZFMNE3551 in the middle of the southern bay.

None of the mylonite localities that are been marked in Stålhös (1989) were found during the field investigations for this project. A possible reason for this is the change in outcrop visibility between 1989 and 2021. Farmlands and modern infrastructure may have obscured any outcropping mylonites. The few localities visited did not yield any strong evidence for the reason behind this topographic low.

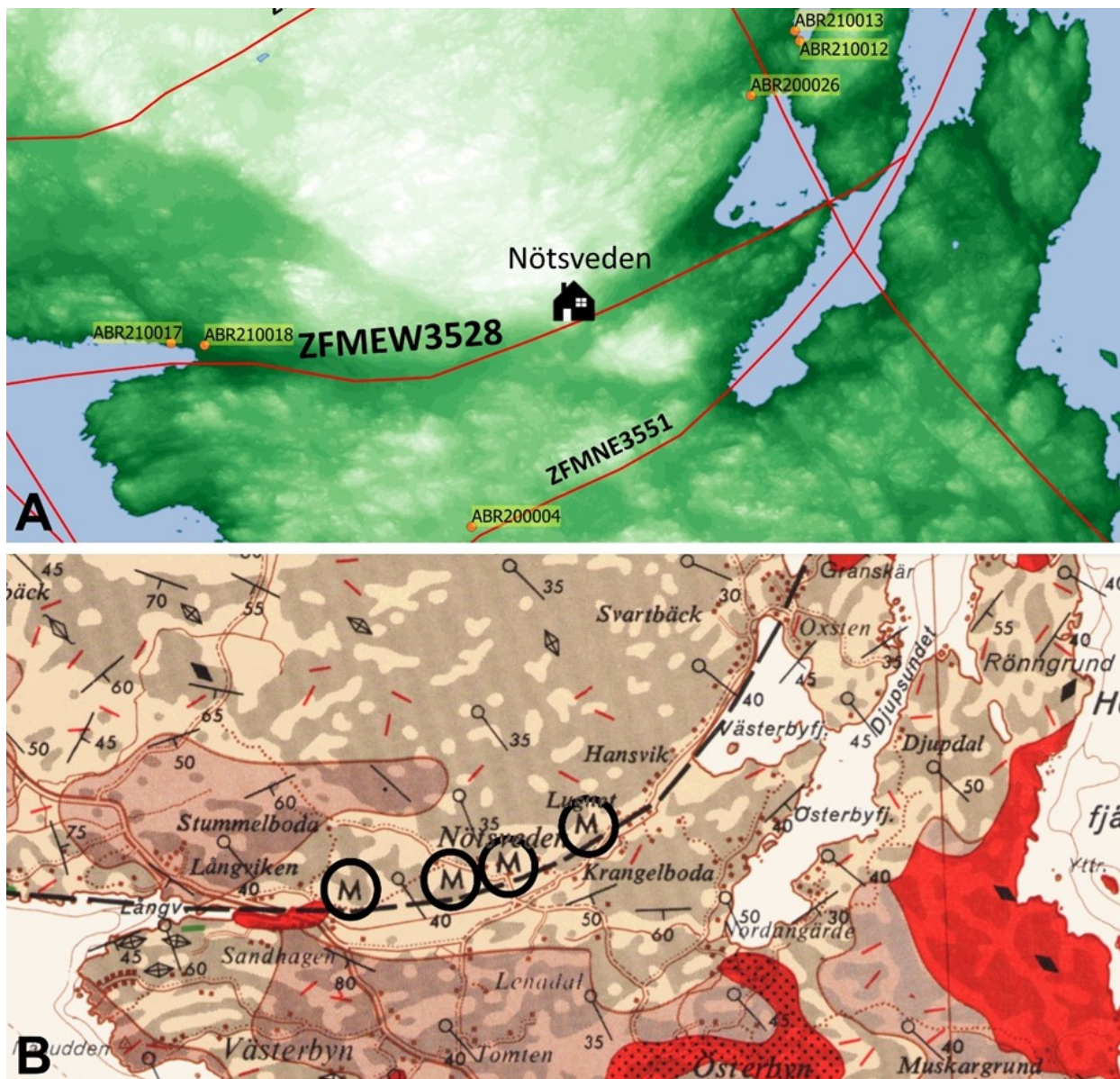


Fig. 4.22. Detail of southern Gräsö A. The Lantmäteriet digital elevation model and lineaments marked. In the middle around the town Nötsveden. B. Original map from Stålhös (1989) with the four mylonite localities 'M' marked.

5 Interpretation and Discussion

5.1 Deformation zone characteristics, kinematics, and fracture minerals

The deformation zones found during the two-stage fieldwork process share distinct characteristics. In sections 4.1 and 4.2, the zones were described from field observations based on their strike, following the example of table 2 in Stephens et al. (2015). The deformation zones described in sub-section 4.1.1, which are located south of the Singö deformation zone, are interpreted to be splays from the Singö zone located in an area inferred to be affected by higher ductile strain (Stephens et al. 2007). The deformation zones described in sub-section 4.1.2 are located inside a tectonic lens north of the Singö zone (Stephens et al. 2007) and are interpreted to cut through this lens. In this section, each group of deformation zone are described and interpreted. The displacements

interpreted occur within the (sub)horizontal plane unless otherwise specified.

5.1.1 Splays from the Singö deformation zone

The Singö deformation zone (SDZ, ZFMWNW0001) is a several hundred metres wide deformation zone with an original dextral sense of shear (Fig. 5.1). As part of the expanded deformation zone model, several lineaments identified by Isaksson & Johansson (2020) are interpreted to be splays from the overall WNW-ESE striking SDZ. For two of these splays (ZFMNW3544 and ZFMNW3545), observations of deformation zones were found in correspondence with the lineaments.

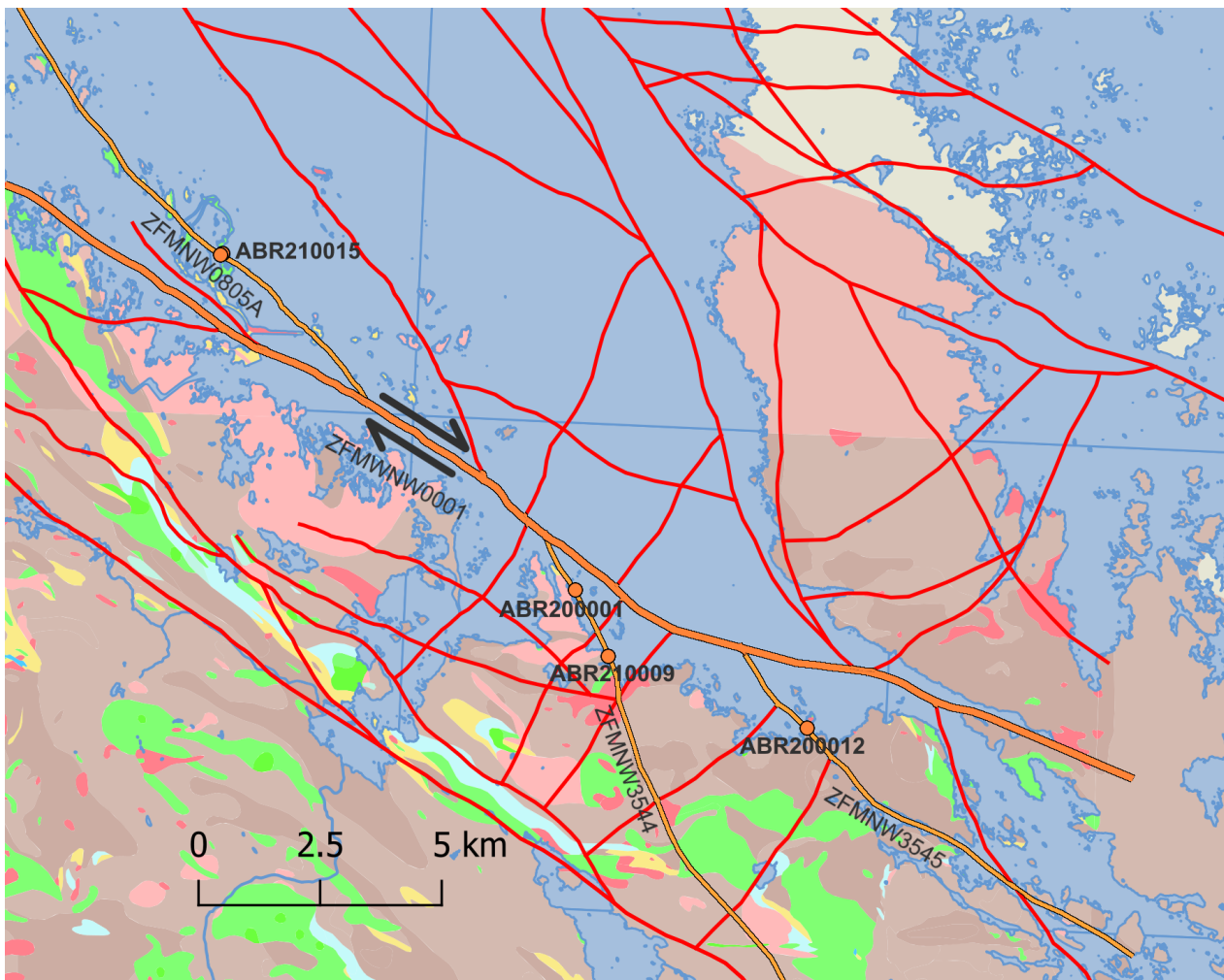


Fig. 5.1. Map showing the Singö deformation zone (ZFMWNW0001) within the revised lineament model by Petersson & Hultgren (2021, in prep.). The ZFMNW3544 and ZFMNW3545 lineaments have been verified by field observations at the marked localities (orange dots). ZFMNW0805A is a Singö splay inside the regional model area of Forsmark. The width of the lineaments is not to scale.

For deformation zone ZFMNW3544 (Figs. 4.1 and 4.2), the outcrop at ABR200001 (table 4.3) is about 1.2 kilometres away from its intersect point with ZFMWNW0001, the outcrop at ABR210009 is about 2.8 kilometres away. One could argue that the outcrop at ABR210009 is not the direct continuation of the same deformation zone found in ABR200001: despite similar trend they differ in other characteristics. The mylonites found at ABR200001 are relatively wide (1.5 – 2 m) in comparison to ABR210009, and the outcrop hosts a sealed breccia (Fig. 4.3B) containing mylonitic clasts. This observation suggests brittle reactivation of a ductile deformation zone. Ductile deformation zones typically act as natural zones of weakness to which subsequent deformation is preferentially localized. The outcrop corresponding to stop ABR210009 lacks brecciation.

The deformation zone at ABR210009 displays kinematic indicators, which are absent at ABR200001. Since the mylonites at ABR210009 cross-cut both foliation and pegmatitic veins, a reconstruction of displacement can be assessed (Fig. 5.2). The wide NW-SE striking and most prominent mylonite has a dextral sense of shear. There are also several splays

from a 010-190-striking mylonite present. The splays are also observed to have a dextral sense of shear, while the main 010-190 striking mylonite shows sinistral displacement. This could be attributed to a local change in main stress (σ_1) direction from roughly NNW-SSE to NE-SW (Fig. 5.3). A field relation between the two different trending mylonites has not been observed. Assuming the mylonites were formed in the same timeframe, the NW-SE and N-S striking ones can be interpreted as conjugate sets.

The contact between the foliated host rock and the ultramylonite seems macroscopically distinct for both ABR200001 and ABR210009: there is no typical gradation of host rock \rightarrow proto-mylonite \rightarrow mylonite \rightarrow ultramylonite. This indicates localized stress.

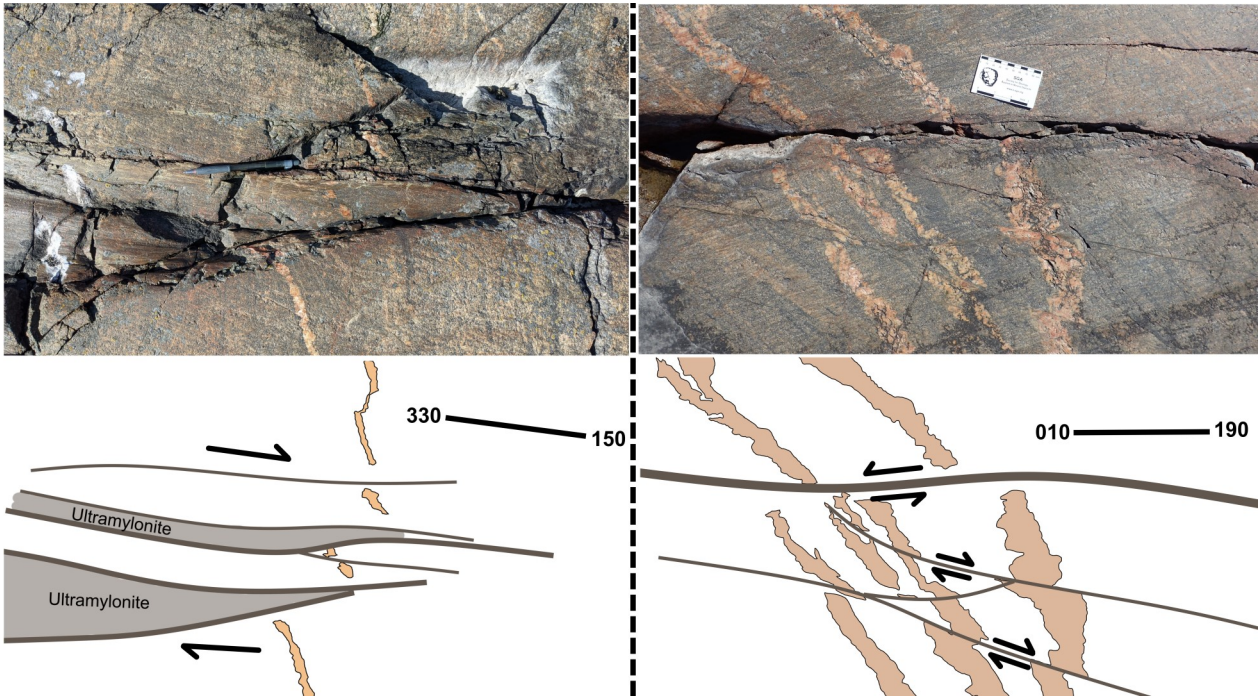


Fig. 5.2. ABR210009: Details of mylonites. A. Ultramylonites varying in width with a NW-SE strike dextrally displace a quartz & feldspar-rich vein with a horizontal displacement of 20 cm. B. Thinner ultramylonite with a NNE-SSW strike sinistrally displaces a quartz & feldspar-rich vein around 10 cm. The brittle fracture does prominent in this figure does not correspond directly to the ultramylonite fabric. Splay mylonites originating from main N-S striking one show varying degrees of dextral displacement.

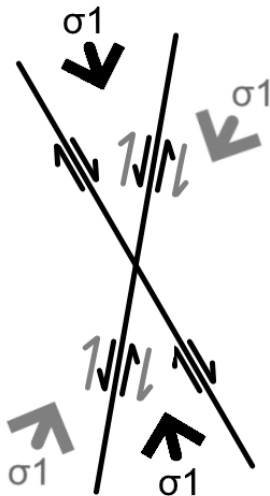


Fig. 5.3. Model of local change in main stress (σ_1) with resulting shear sense in NW-SE and roughly N-S striking mylonites.

The mylonite and breccia of ZFMNW3545, visible at ABR200012 (Fig. 4.5), are about 2150 m to the southwest of its junction with the Singö zone. Just like ABR200002, the breccia contains mylonitic clasts (Fig. 4.5). This reaffirms brittle reactivation of ductile deformation zones. There are also a few 020-200 striking fractures with a sinistral sense of shear, implied from horizontal displacement of the 135-315 striking mylonite (Fig. 5.4). It is unsure whether there is a vertical slip component present in these 020-200 striking fractures.

At outcrop ABR210015, a NW-SE striking splay from the Singö zone intersects with an outcrop inside the Forsmark regional model area. This intersection is about 4.2 kilometres away from its intersect point with the Singö zone. A NW-SE striking protomylonite (Fig. 5.5A) accompanied by an NNE-SSW striking mylonite (Fig. 5.5B) are present at this locality, the same strikes as found in ABR210009. There is a gradation from a proto- to an ultramylonite visible in the NW-SE trending zone.

In conclusion, the deformation zones which are interpreted to be splays from the Singö deformation zone are characterized by NW-SE striking zones with a dextral sense of shear. These zones consist locally of both a ductile and brittle component, the latter containing clasts with a ductile fabric. The width of each mylonite and breccia varies, from centimetre- to metre-scale. Locally, roughly N-S striking fractures with a sinistral sense of shear are also present, both ductile and brittle in nature. At locality ABR210009, splays from a N-S striking ultramylonite have a dextral sense of shear. A local change of main stress direction can be interpreted for this locality.

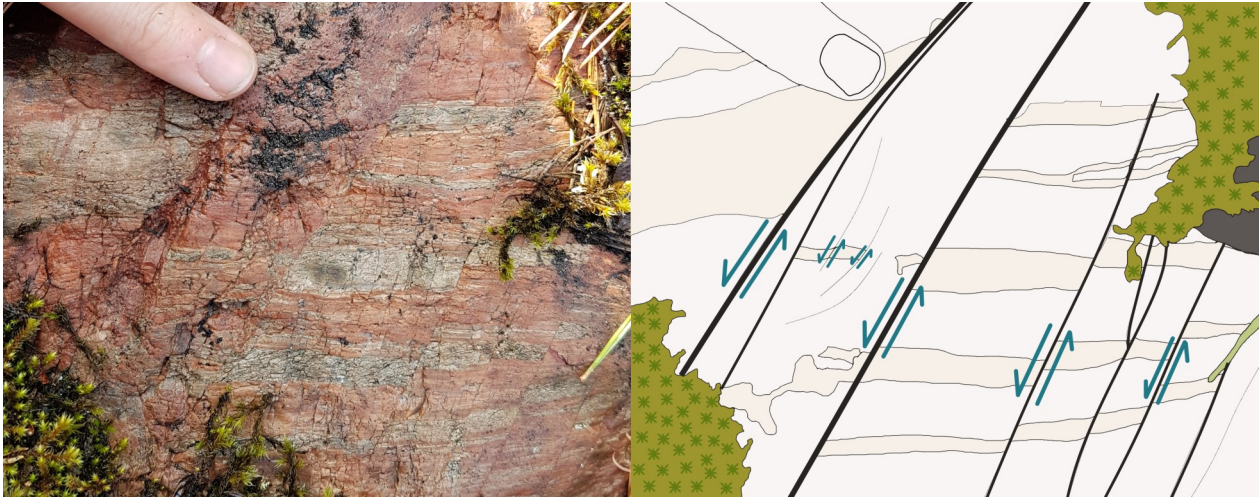


Fig. 5.4. ZFMNW3545: 020-200 striking fractures that sinistrally displace the mylonitic fabric. Strike-slip direction of the big fracture is unclear from field observations, but assumed to be the same as the smaller fractures.

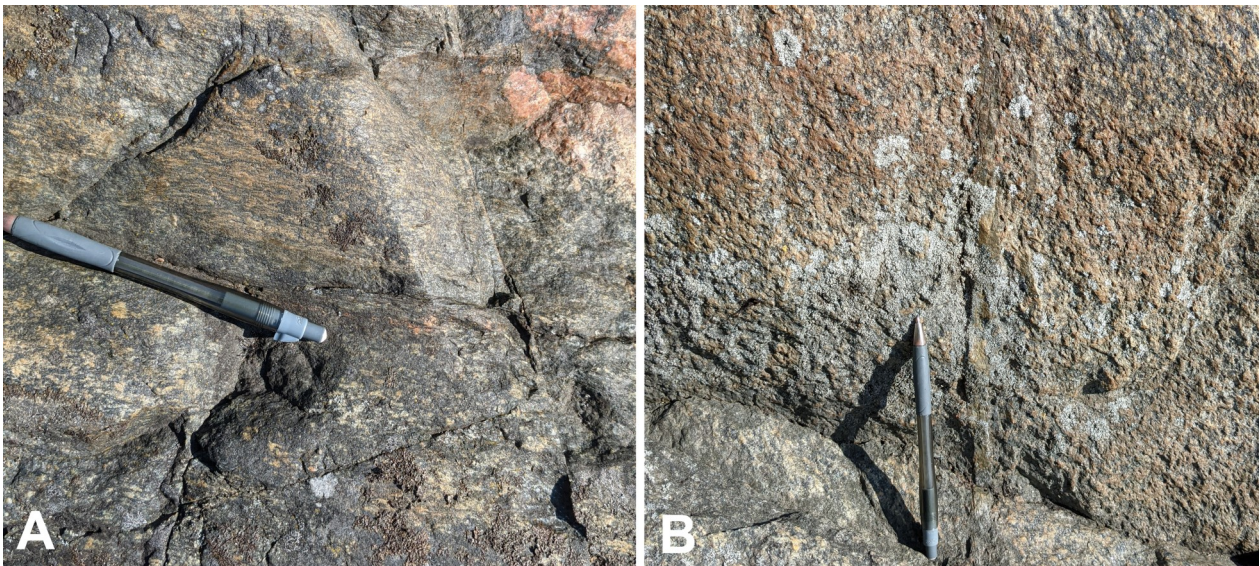


Fig. 5.5. ABR2100015: A. NW-SE trending mylonite, photo taken from the top. B. NNE-SSW trending mylonite, photo taken from the side.

5.1.2 NW-SE and NNW-SSE striking deformation zones of central Gräsö

The lineaments ZFMNW3511 and ZFMNW3519 intersect at two places below sea level (Fig. 5.6). The two lineaments form the northern and southern border to an eye-shaped tectonic lens. Both lineaments coincide with long and broad topographical depressions. ZFMNW3511 runs from Väster-Mörtarövik in the west to Mörtaröfjärden in the east. At the western shore, the lineament could be verified as a wide, heavily fractured and red-stained deformation zone. Further inland and to the eastern shore, farmlands cover the lineament almost entirely along its extent. Outcrops are sparse in these areas, and show a lower intensity of fractures than in the western outcrops. Near the southern border of the lineament, at locality ABR200021 on the western shore (Fig. 4.8B), a very fine-grained to glassy banded rock is found, interpreted as a mylonite or ultrabreccia. All other localities corresponding to lineament ZFMNW3511 host a heavily fractured rock with brecciated veins

(Fig. 4.9A, B), locally with vugs (Fig. 4.10A, B). ZFMNNW3533 is observed in two localities, of which the southern one (ABR200027) is the largest and poses the best overview of the deformation zone. The fractured rock of ABR200027 is similar in appearance with outcrops along the road from Väster- to Öster-Mörtarö. The triple point where ZFMNNW3533 meets ZFMNW3511 (depicted by a question mark in figure 5.6) is not visible in the field, so their relationship remains uncertain.

Lineament ZFMNW3519 could not be verified during field work: there were no viable outcrops visible from orthophotos in the low-lying inland and the rocky shores at the western part of the island were surrounded by impassable swamps. Even with no direct field evidence, the geophysical and topographical data strongly suggest that ZFMNW3519 is another major NW-SE zone parallel to ZFMNW3511.

On deformation zone maps from SGU (Fig. 2.6), both ZFMNW3511 and ZFMNW3519 are already drawn, although not in the exact same place, and

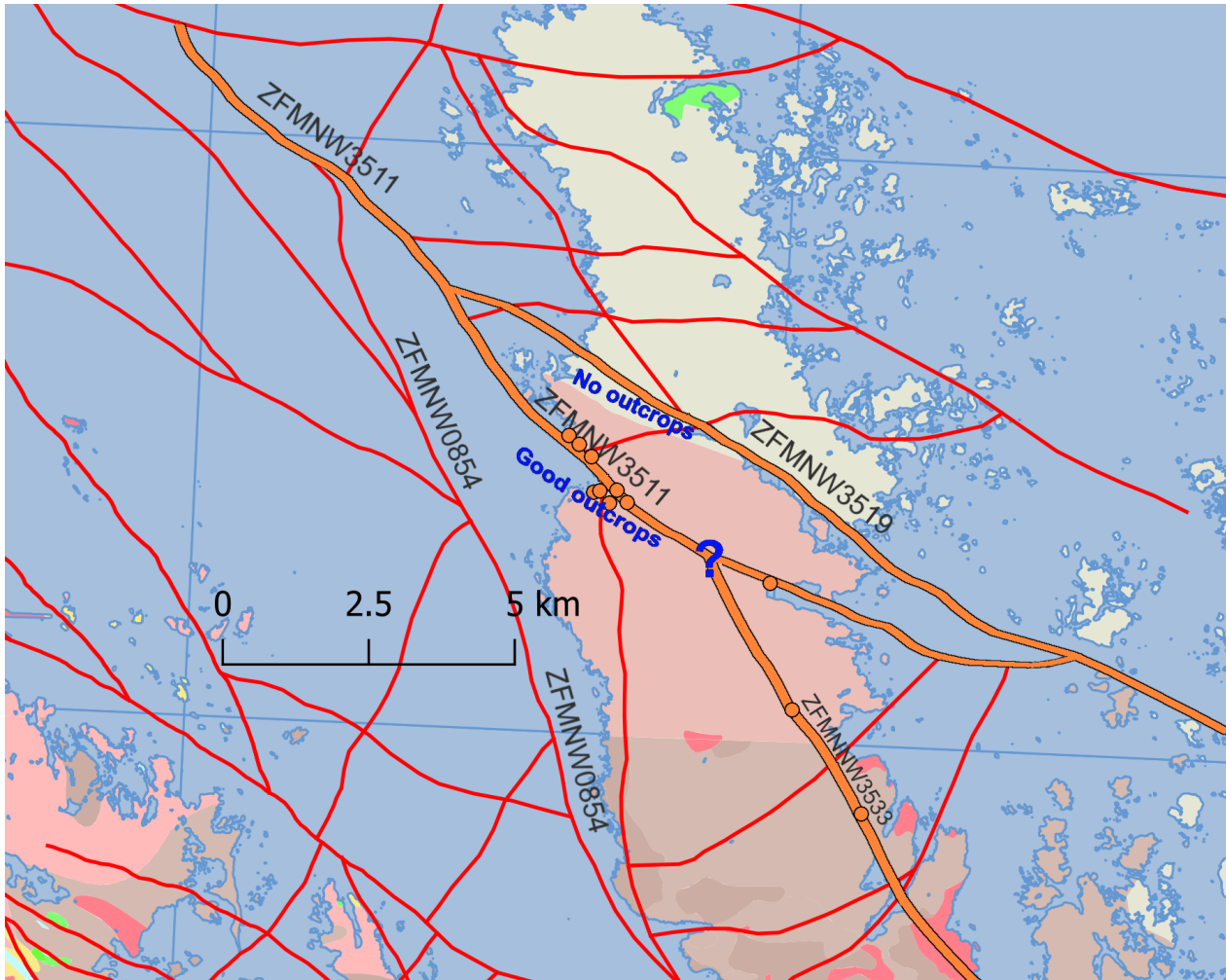


Fig. 5.6. Map showing the NW-SE and NNW-SSE trending lineaments at central Gräsö within the revised lineament model by Petersson & Hultgren (2021, in prep.). ZFMNW3511 & ZFMNNW3533 are verified lineaments based on field observations from the marked stops. ZFMNW3519 is a high-confidence lineament not visible in the field. The width of the lineaments is not to scale.

classified as purely brittle deformation zones. The differences between the SGU data and my observations are the ductile component in ZFMNW3511, visible at locality ABR200021 and the more upwards curve of the zone at the western shore, closely following the northern coastline of the bay inlet.

On the same map (Fig. 2.6), a straight deformation zone is drawn just west of the western shoreline of Gräsö. This could represent lineament ZFMNW0854, a high-confidence lineament which coincides with a broad magnetic minimum. Since this lineament is entirely below sea level it could not be verified during field work.

5.1.3 E-W (080-260) striking deformation zones

While exploring the outcrops at the western shore of Gräsö, some purely brittle deformation zones were discovered (Fig. 4.15). Their roughly E-W strike (080-260) is rare in the Forsmark regional model, version 2.3 (Stephens & Simeonov 2015). Common fracture minerals observed in the field are hematite-stained and filled by adularia and laumontite and calcite (Fig. 5.8). The hematite-stained fracture minerals occur as sub-

mm sized crystals while the calcite often occurs in large aggregates with idiomorphic crystals. At locality ABR200014, a chlorite or epidote coating has been observed on a fracture plane wall rock.

The clearest evidence of the 080-260 trending zones is at locality ABR200016, where several semi-parallel brittle zones clearly crosscut the tectonic foliation of the surrounding host rock (Fig. 4.20). No sense of shear is apparent when looking at the undeformed lenses between the undulating fine-grained fault gauges.



Fig. 5.8. ABR200014: Detail of border of main brittle deformation zone oriented 265/85. The light orange and darker red fine-grained fault core consists mostly of hematite-stained laumontite and adularia. The milky white grains are calcite aggregates.

5.2 Tectonic development and paleostress reconstruction

Numerous papers and SKB reports describe the tectonic development of the regional area around the planned repository, especially within the tectonic lens. One of the research questions as stated in the introduction is whether the deformation zones in the expanded area on Gräsö and along the Öregrund coast can be explained with the tectonic models made for the regional area. To answer this question, the observations and interpretations described in chapter 4 and section 5.1 must be addressed. The strike, kinematics, cross-cutting relationship and fracture minerals are the key data used in this discussion.

The kinematic data of the verified Singö splay zones ZFMNW3544 and ZFMNW3545 fit well within the current tectonic model: the NW-SE trending zones have been formed in a ductile regime and displace older pegmatitic veins with a dextral sense of movement in the horizontal plane (Fig. 5.9). Adjacent N-S and NNE-SSW striking zones display both sinistral and dextral strike slip movement (Fig. 5.9). The black arrows in figure 5.9 of the main stress model would correspond to roughly N-S compression during the Svecokarelian orogeny (Stephens & Wahlgren 2008; Saintot et al. 2011). The red arrows could correspond to a local change in main stress to a more NNE-SSW direction. According to Stephens et al. (2015), a local variance to a more NNE-SSW oriented stress occurs between the Singö deformation zone and the Eckarfjärden deformation zone around and after 1.8 Ga (Fig. 5.9). It is hypothesized that the transition from ductile to brittle deformation happened between 1.8 and 1.7 Ga, based on 40Ar–39Ar biotite cooling ages (Söderlund et al. 2008). The breccias found along the NW-SE trending zones ZFMNW3544 and ZFMNW3545 are thus interpreted to have formed after ca. 1.7 Ga.

The NW-SE striking deformation zones ZFMNW3511 and ZFMNW3519 in central Gräsö are much wider than the Singö splays and are almost completely brittle in nature. This may be due to the fact that the central Gräsö area is not in an area inferred to have been affected by high ductile strain (Stephens et al. 2007; Saintot et al. 2011) (Fig. 2.3). As the crystalline basement presumably was in a ductile regime before 1.7 Ga (Söderlund et al. 2008), these deformation zones would have been formed within in the same time frame as the Singö deformation zone and its splays, with an inferred dextral sense of shear. Extensive brittle reactivation around the zone is inferred to have formed after 1.7 Ga with a sinistral sense of shear. However, no displacement of any kind has been observed in the field, due to the lack of tectonic markers.

One interesting result of this study was the discovery of relatively wide (10–40 m) ~080–260 striking steeply dipping brittle deformation zones on Gräsö and one in the high strain area in the northwestern corner of Öregrund. Zones having the same strike and fracture characteristics have not been described in previous studies of the regional Forsmark area. The fracture mineral assemblage consisting of calcite and hematite-stained adularia and laumontite indicates that they belong to a second generation of fracture minerals, possibly linked to the Sveconorwegian orogeny (Sandström et al. 2009) (Fig. 2.5). In figure 4.18, a brittle fracture zone with a 080–260 degree strike is interpreted to be the youngest and have a dextral sense of shear. This displacement would fit in the tectonic model for the Sveconorwegian orogeny affecting the Forsmark area, where ENE–WSW compression is interpreted (Stephens & Wahlgren 2008; Saintot et al. 2011). In none of the other ± 080–260 trending brittle zones is field evidence found for displacement. This could be due to the extensional nature of these characteristic fracture zones. According to the tectonic model for Forsmark

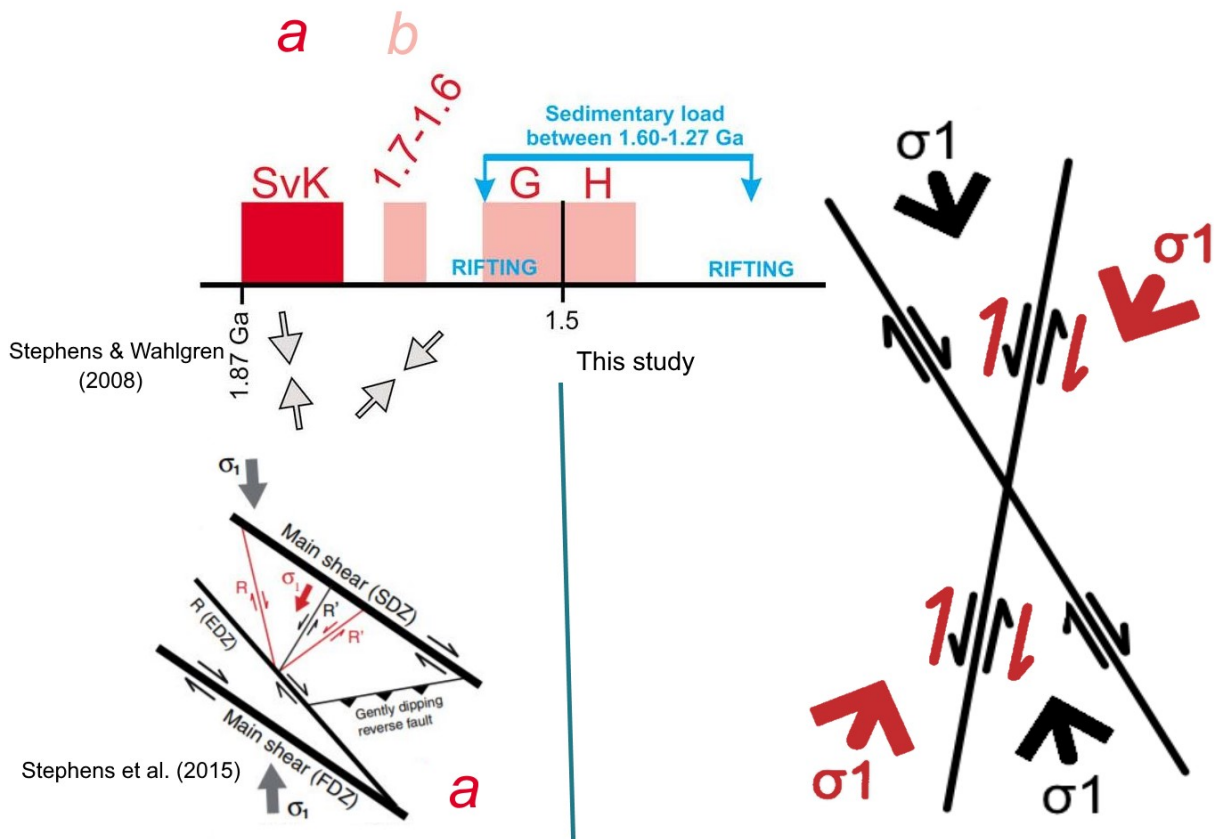


Fig. 5.9. Rotation of main stress direction (σ_1) from roughly N-S to ENE-WSW between the SDZ and EDZ during the Svecokarelian orogeny. The tectonic model to the left is modified from Stephens & Wahlgren (2008) (ages of orogenies and rifting) and Stephens et al. (2015), modified after Saintot et al. (2011) (model of main stress directions and consequently shear sense of discrete deformation zones). The model to the right is from this study.

by Stephens et al. (2015), no new zones are formed after 1.8 Ga. This study suggests however that the ~080-260 striking zones are zones formed after 1.8 Ga since they are purely brittle in nature and have a strike that is not represented by the Svecokarelian model (Stephens et al. 2015). One of the fracture planes of a 080-260 striking zone at locality ABR200014 is coated in epidote and/or chlorite (Fig. 5.10A). These are fracture minerals commonly associated with fractures formed during older orogenies (Sandström et al. 2009) (Fig. 2.5). It is possible, however, that these fracture minerals precipitated during the 1.1-0.9 Ga Sveconorwegian orogeny (Sandström et al. 2009) (Fig. 2.5). A quartz vein is seemingly both crosscutting and being sinistrally displaced by a 080-260 striking brittle zone in locality ABR200014 (Fig. 5.10B). They could both have been formed during the early Sveconorwegian and later gradually sinistrally reactivated as a result of far-field orogenic stress. The main issue with the newly discovered brittle zones is that they do not show on the low-resolution magnetic maps from SGU, from the VLF maps, and on the digital elevation models from Lantmäteriet. Further investigation of these zones is recommended.

According to Sandström et al. (2009), this fracture mineral assemblage is typical for deformation linked to the c. 1.1-0.9 Ga Sveconorwegian orogeny (Fig. 2.5) and is similar to the abovementioned ~080-260 striking zone assemblage.

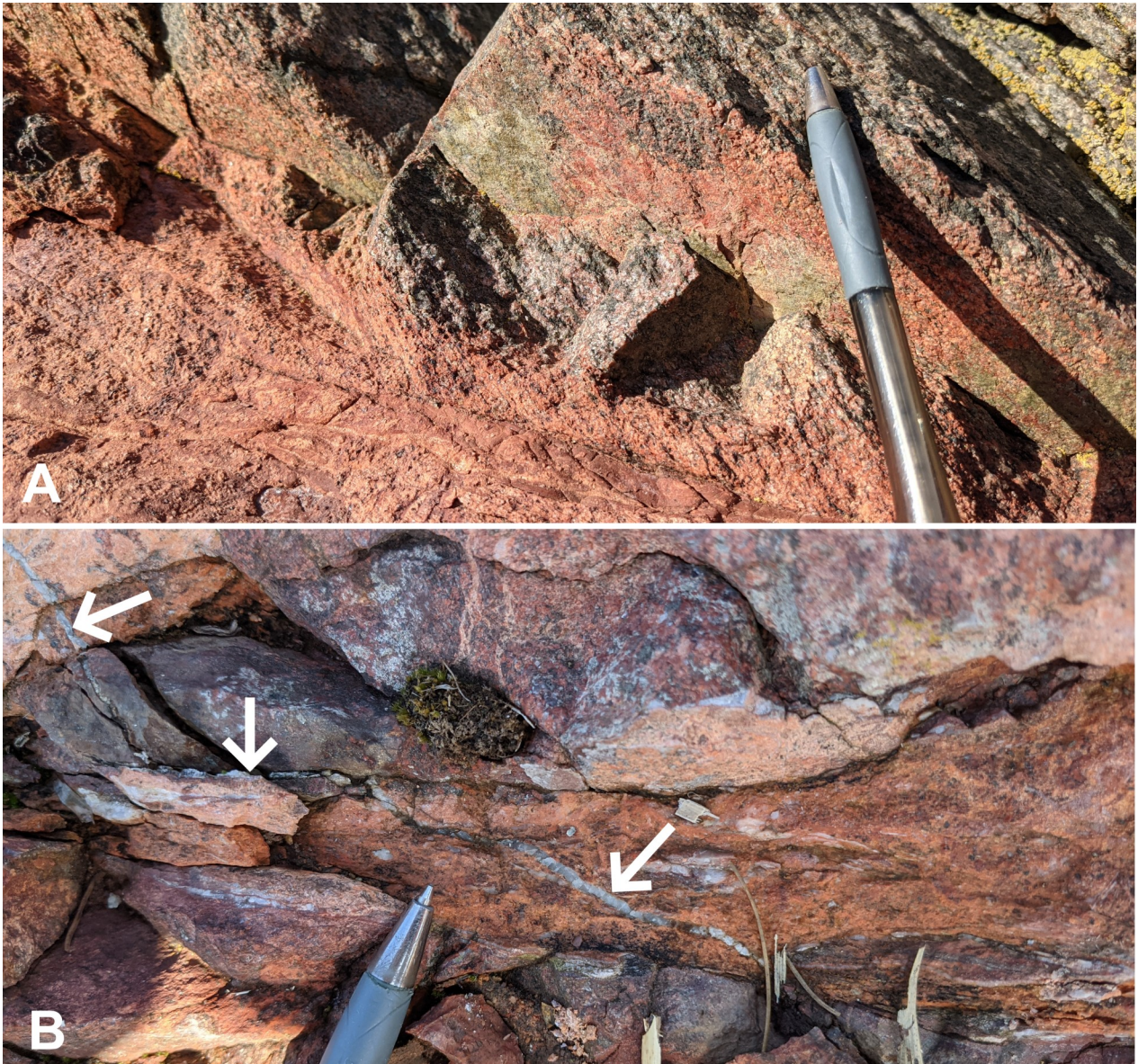


Fig. 5.10. ABR20014: **A.** Epidote or chlorite coating (green coloured minerals) on vertical fracture plane at the contact between a fine-grained red-stained 080-260 striking brittle fracture zone and the crystalline host rock. **B.** A NW-SE striking quartz vein simultaneously cross-cutting and being displaced by a fine-grained red-stained 080-260 striking brittle fracture zone. White arrows point to the quartz vein and are perpendicular to its strike.

5.3 Relationship between general structural grain and lineaments

In between ZFMNW3519 and ZFMNW3511, the bedrock data from SGU shows the contact between metamorphosed granitoid rock and orthogneisses (Fig. 5.11A). At this boundary, it is then supposed that the rocks in the north have been subjected to a higher strain rate. The contact between these two main rock types has a NW-SE trend, parallel to the one main set of lineaments. When looking at the digital elevation model from Lantmäteriet (Fig. 5.11B), it is clear that the centre of Gräsö is a topographic high compared to the northern area. There are topographic lows that coincide with tectonic lineaments, most obvious the NW-SE trending lineaments in the middle of the island.

There are several E-W trending lineaments to the north of ZFMNW3519: ZFMEW3512, ZFMEW2323, ZFMEW3513 and ZFMEW3514 (Fig. 5.13A). None of these correlate with deformation zones, as discovered in this project and in an independent field study by Jesper Petersson in march 2021. Instead, the lineaments were mostly found to be parallel to the structural grain of the gneissic rocks. In the very north of Gräsö, the metaintrusive rocks are deformed in a more intense ductile regime. The structural grain appears to be reflected in the digital elevation model (Fig. 5.12A). The E-W trending lineament ZFMEW3512 is inferred to also represent the gneissosity, from two localities: ABR200024, where the gneissic foliation strikes 100 and ABR200030 where the foliation strikes 095 (Fig. 5.12B). The NW-trending lineament ZFMNW3520 is visited in one locality (ABR200025) (Fig. 5.12B). Here, the gneissic

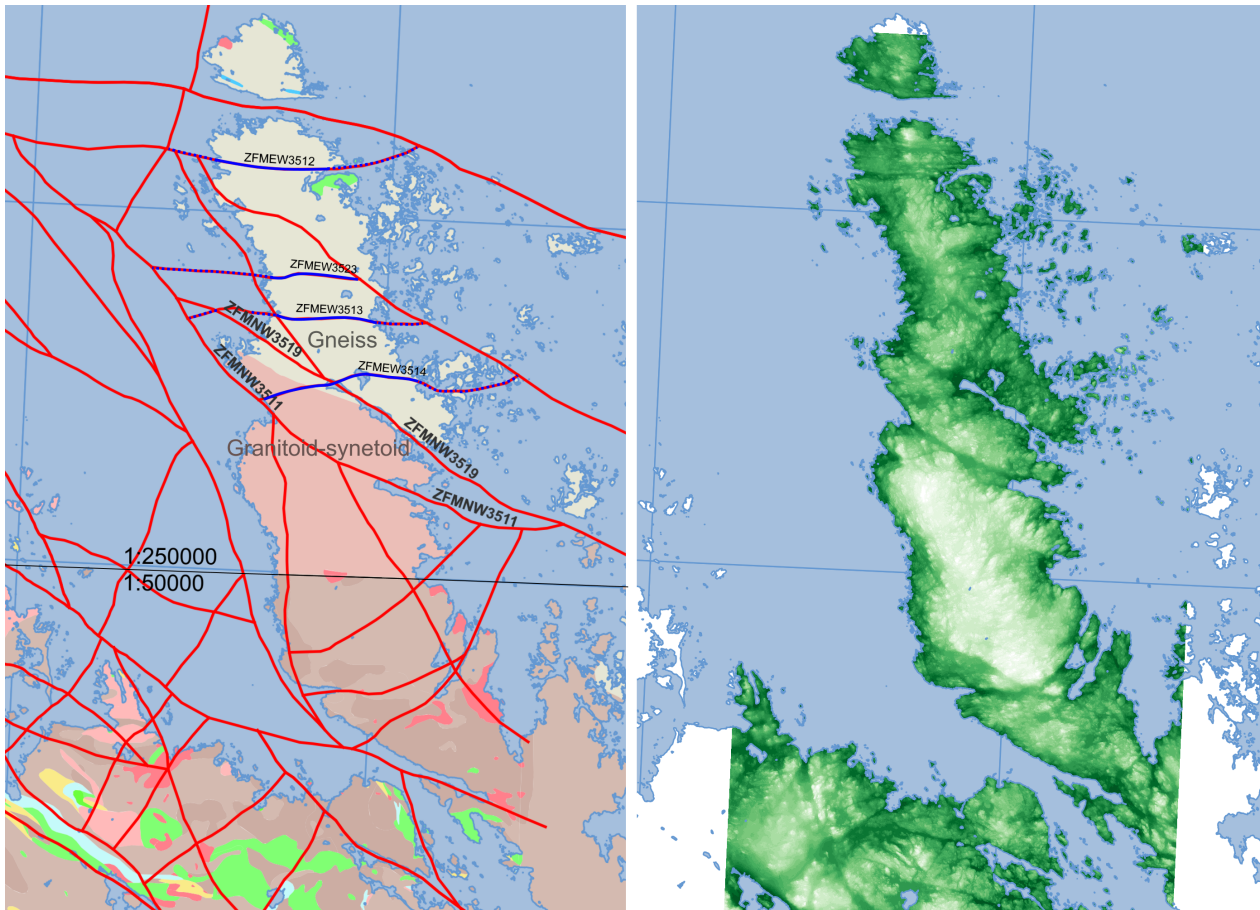


Fig. 5.11. Gräsö rock units and elevation, showing **A**. The division between the originally 1:250000 scale bedrock map in the north and the originally 1:50000 scale map in the south is depicted on the SGU bedrock basemap. It also shows the two lineaments ZFMNW3519 and ZFMN3511 in between which the division between the granitoid-synetoid system in the south and the gneiss system in the north is located. Lineaments in blue are the E-W trending lineaments which are mostly parallel to the structural grain. **B**. Lantmäteriet digital elevation model of Gräsö and part of the Swedish mainland in the south.

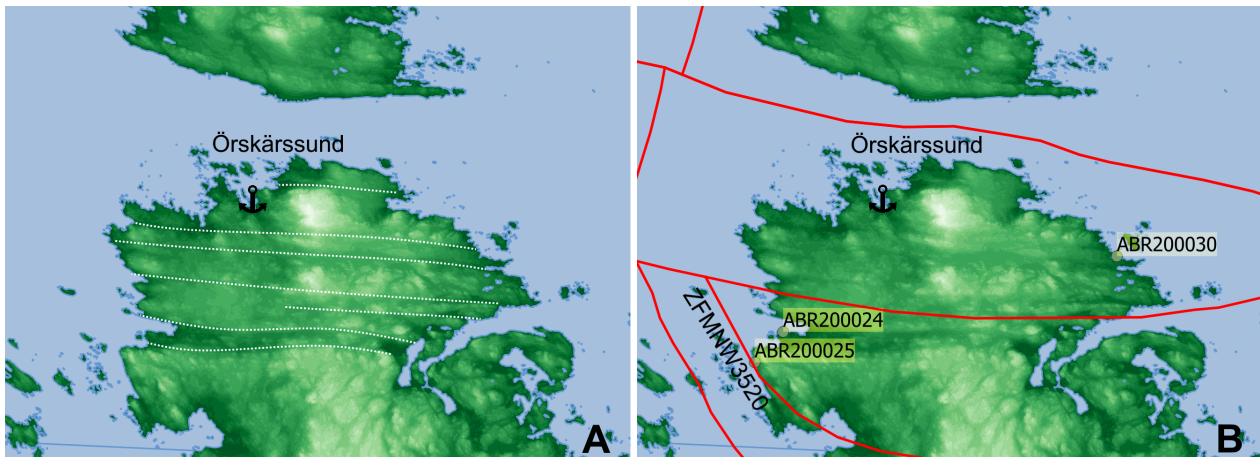


Fig. 5.12. **A**. Lantmäteriet elevation basemap of northern Gräsö showing E-W bands of lower elevation (white dotted lines). **B**. The same elevation basemap superimposed by stage 2 interpreted lineaments (Isaksson & Johansson 2020 and subsequently revised by Petersson & Hultgren 2021, in prep.).

foliation strikes 140 (Fig. 5.13). With no field evidence for a deformation zone, it is likely that the structural grain is responsible for this lineament as well.



Fig. 5.13. View facing north at locality ABR200025 (6708796 N, 0170206 E), intersecting with lineament ZFMNW3520. Orthogneiss with alternating felsic and mafic banding that strikes to 140.

6 Conclusions

1. NW-SE striking deformation zones linked to the Singö deformation zone (ZFMNW3544, ZFMNW3545) show strong ductile deformation and highly localized mylonitisation. They are locally overprinted by brittle deformation. These zones show dextral strike-slip displacement, locally with possible conjugate N-S and NNE-SSW striking mylonites with a sinistral and dextral sense of shear, which is in agreement with the tectonic concept of Stephens et al. (2015) which was developed for the Forsmark area. The zones lie within an area affected by high strain (Stephens et al. 2007). Following the cooling history by Söderlund et al. (2008), these zones were probably formed before 1.8 Ga and continuously reactivated around and after 1.8 Ga.

2. NW-SE and NNW-SSE striking deformation zones cutting through Central Gräsö (ZFMNW3511, ZFMNW3519, ZFMNNW3533) have formed within a low-strain rock volume outside the Forsmark tectonic lens (Stephens et al. 2007). They form wide highly fractured zones, characterized by red-stained breccias, locally sealed with quartz vein networks and vuggy quartz. The observations of mylonites show that these zones were first formed under relatively high temperatures and later reactivated during lower temperatures.

3. Roughly E-W (080-260) striking, steeply dipping brittle zones are associated with fracture mineral assemblages of calcite-laumontite-adularia, which is indicative of possibly extensional fractures linked to the 1.1-0.9 Ga Sveconorwegian orogeny (Sandström et al. 2009). This study suggests that these zones are not reactivated zones that were formed before 1.8 Ga but rather young purely brittle zones,

extensional in nature.

4. Geophysical lineaments interpreted by Isaksson & Johansson (2020) in the northern parts of Gräsö where the bedrock consists of banded orthogneisses do not seem to be indicative of deformation zones or any defined well-defined zone of localized strain. Instead, these lineaments are found to be roughly parallel to the tectonic foliation in the gneiss rock.

7 Acknowledgements

I have been given a unique opportunity to work in this fascinating area as my master project, with the help of a lot of incredible people I have met during the process. Firstly, I would like to thank Charlotte Möller (LU) for recommending me as an aspiring structural geologist to SKB after I expressed my interest for the geological storage of nuclear waste. Secondly, I would like to thank Susanne Grigull (SKB) for her continuous support and guidance in the field and during my writing process and her excellent guidance of the SKB-drone in stressful conditions. I am also very grateful for her hospitality during my stay in Stockholm. I would like to thank Jesper Petersson (GEOS) and Peter Hultgren (SKB) for helping me in the beginning of this project and as guides during the field introduction. Next, I would like to thank Mathias Andersson (SKB) for helping Susanne and me with the drone operations and for preparing orthomosaics for me. SKB has been so generous to cover my travel and accommodation expenses during the two field work periods. From Lund University, I would like to thank my supervisor Ulf Söderlund for his helpful comments in the late stage of this project. Lastly, I would like to thank my friends Märta Westberg and Per Wahlquist for their company and support.

8 References

Agisoft Metashape Professional (Version 1.7.2) (Software). (2021). Retrieved from <http://www.agisoft.com/downloads/installer/>

Long-term safety for the final repository for spent nuclear fuel at Forsmark. Main report of the SR-Site project. SKB TR-11-01, Svensk Kärnbränslehantering AB.

Andersson J., 2003. Site descriptive modelling – strategy for integrated evaluation. SKB R-03-05, Svensk Kärnbränslehantering AB.

Bergman S., Isaksson H., Johansson R. (ed), Lindén A., Persson C., Stephens M., 1996. Förstudie Östhammar. Jordarter, bergarter och deformationszoner. SKB PR D-96-016, Svensk Kärnbränslehantering AB.

Bergman T., Johansson R., Lindén A. H., Rudmark L., Stephens M., Isaksson H., Lindroos H., 1999. Förstudie Tierp. Jordarter, bergarter och deformationszoner. SKB R-99-53, Svensk Kärnbränslehantering AB.

Bergman, S., Stephens, M.B., Andersson, J., Kathol, B. & Bergman, T., 2012. Sveriges berggrund, skala 1:1 miljon [Bedrock Map of Sweden, Scale 1:1 Million]. Sveriges geologiska undersökning K423.

Beunk, F.F. & Kuipers, G., 2012. The Bergslagen ore province, Sweden: review and update of an accreted orocline, 1.9–1.8 Ga BP. *Precambrian Research*, 216–219, 95–119, <https://doi.org/10.1016/j.precamres.2012.05.007>

Curtis P., Markström I., Petersson J., Triumf C-A., Isaksson H., Matsson H., 2011. Site investigation SFR. Bedrock geology. SKB R-10-49, Svensk Kärnbränslehantering AB.

Hermansson, T., Stephens, M.B., Corfu, F., Andersson, J., Page, L., 2007. Penetrative ductile deformation and amphibolite-facies metamorphism prior to 1851 Ma in the western part of the Svecofennian orogen, Fennoscandian Shield. *Precambrian Res.* 153, 29–45.

Hermansson, T., Stephens, M.B., Corfu, F., Page, L.M., Andersson, J., 2008a. Migratory tectonic switching, western Svecofennian orogen, central Sweden: Constraints from U/Pb zircon and titanite geochronology. *Precambrian Research* 161, 250–278. <https://doi.org/10.1016/j.precamres.2007.08.008>

Hermansson, T., Stephens, M.B., Page, L.M., 2008b. ⁴⁰Ar/³⁹Ar hornblende geochronology from the Forsmark area in central Sweden: Constraints on late Svecofennian cooling, ductile deformation and exhumation. *Precambrian Research* 167, 303–315. <https://doi.org/10.1016/j.precamres.2008.09.003>

Högdahl, K., Sjöström, H. & Bergman, S. 2009. Ductile shear zones related to crustal shortening and domain boundary evolution in the central Fennoscandian Shield. *Tectonics*, 28, TC1003, <https://doi.org/10.1029/2008TC002277>

Isaksson, H., Keisu, M., 2005. Interpretation of airborne geophysics and integration with topography. Stage 2 (2002-2004). Forsmark site investigation. Swedish Nuclear Fuel and Waste Management Company, Stockholm, Report P-04-282 (76 pp. <http://www.skb.se/publications>).

Isaksson, H., Thunehed, H., Pitkänen, T., Keisu, M., 2007. Detailed ground magnetic survey and lineament interpretation in the Forsmark area, 2006–2007. Forsmark site investigation. Swedish Nuclear Fuel and Waste Management Company, Stockholm, Report R-07-62 (48 pp. <http://www.skb.se/publications>).

Jansson, N.F., Zetterqvist, A., Allen, R.L., Billström, K. & Malmström, L., 2017. Genesis of the Zinkgruvan stratiform Zn–Pb–Ag deposit and associated dolomite-hosted Cu ore, Bergslagen, Sweden. *Ore Geology Reviews*, 82, 285–308, <https://doi.org/10.1016/j.oregeorev.2016.12.004>

Jansson, N.F., 2017. Structural evolution of the Palaeoproterozoic Sala stratabound Zn–Pb–Ag carbonate-replacement deposit, Bergslagen, Sweden. *GFF*, 139, 21–35, <https://doi.org/10.1080/11035897.2016.1196498>

Kampmann, T.C., Stephens, M.B. & Weihed, P., 2016. 3D modelling and sheath folding at the Falun pyritic Zn–Pb–Cu–(Au–Ag) sulphide deposit and implications for exploration in a 1.9 Ga ore district, Fennoscandian Shield, Sweden. *Mineralium Deposita*, 51, 665–680, <https://doi.org/10.1007/s00126-016-0638-z>

Sandström B., Page L., Tullborg E.-L., 2006. Forsmark site investigation. ⁴⁰Ar/³⁹Ar (adularia) and Rb–Sr (adularia, prehnite, calcite) ages of fracture minerals. Report SKB P-06-213. Swedish Nuclear Fuel and Waste Management Co. (SKB). <http://www.skb.se>

Sandström, B., Annersten, H., Tullborg, E.-L., 2008. Fracture-related hydrothermal alteration of metagranitic rock and associated changes in mineralogy, geochemistry and degree of oxidation: a case study at Forsmark, central Sweden. *Int. J. Earth Sci.* <http://dx.doi.org/10.1007/s00531-008-0369-1>.

Sandström, B., Tullborg, E.-L., Larson, S.Å., Page, L., 2009. Brittle tectonothermal evolution in the Forsmark area, central Fennoscandian Shield, recorded by paragenesis, orientation and ⁴⁰Ar/³⁹Ar geochronology of fracture minerals. *Tectonophysics* 478, 158–174. <https://doi.org/10.1016/j.tecto.2009.08.006>

Stephens M. B., Fox A., La Pointe P., Simeonov A, Isaksson H., Hermanson J., Öhman J., 2007. Geology Forsmark. Site descriptive modelling Forsmark stage 2.2. SKB R-07-45, Svensk Kärnbränslehantering AB.

Stephens, M. B., and C.-H. Wahlgren, 2008. Bedrock evolution, in Geological Evolution, Palaeoclimate and Historical Development of the Forsmark and Laxemar-Simpevarp Areas: Site Descriptive Modelling SDM-Site, edited by B. Söderbäck. SKB R-08-19, Svensk Kärnbränslehantering AB.

Stephens, M.B., Ripa, M. et al., 2009. Synthesis of the Bedrock Geology in the Bergslagen Region, Fennoscandian Shield, South-Central Sweden. Sveriges geologiska undersökning Ba58.

Stephens M. B., Simeonov A., 2015. Description of deformation zone model version 2.3, Forsmark. SKB R-14-28, Svensk Kärnbränslehantering AB.

Stephens, M.B., Follin, S., Petersson, J., Isaksson, H., Juhlin, C., Simeonov, A., 2015. Review of the deterministic modelling of deformation zones and fracture domains at the site proposed for a spent nuclear fuel repository, Sweden, and consequences of structural anisotropy. *Tectonophysics* 653, 68–94. <https://doi.org/10.1016/j.tecto.2015.03.027>

Stephens, M.B., 2020. Paleoproterozoic (1.9-1.8 Ga) Migratory accretionary orogeny. In M.B. Stephens & J. Bergman Weihed (eds): Sweden: Lithotectonic Framework, Tectonic Evolution and Mineral Resources, 237 – 250. The Geological Society.

Stephens, M.B. & Bergman, S., 2020. Regional context and lithotectonic framework of the 2.0–1.8 Ga Svecokarelian orogen, eastern Sweden. In M.B. Stephens & J. Bergman Weihed (eds): Sweden: Lithotectonic Framework, Tectonic Evolution and Mineral Resources, 19 – 26. The Geological Society.

Stephens, M.B. & Jansson, N.F., 2020. Paleoproterozoic (1.9-1.8 Ga) Syn-orogenic magmatism, sedimentation and mineralization in the Bergslagen lithotectonic unit, Svecokarelian orogen. In M.B. Stephens & J. Bergman Weihed (eds): Sweden: Lithotectonic Framework, Tectonic Evolution and Mineral Resources, 154 – 206. The Geological Society.

Söderlund, P., Hermansson, T., Page, L.M., Stephens, M.B., 2008. Biotite and muscovite $^{40}\text{Ar}/^{39}\text{Ar}$ geochronological constraints on the post-Svecofennian tectonothermal evolution, Forsmark site, central Sweden. *International Journal of Earth Sciences*. doi:10.1007/s00531-008-0346-8

**Tidigare skrifter i serien
"Examensarbeten i Geologi vid Lunds
universitet":**

571. Persson, Eric, 2019: An Enigmatic Cerapodian Dentary from the Cretaceous of southern Sweden. (15 hp)
572. Aldenius, Erik, 2019: Subsurface characterization of the Lund Sandstone – 3D model of the sandstone reservoir and evaluation of the geoenery storage potential, SW Skåne, South Sweden. (45 hp)
573. Juliusson, Oscar, 2019: Impacts of subglacial processes on underlying bedrock. (15 hp)
574. Sartell, Anna, 2019: Metamorphic paragenesis and P-T conditions in garnet amphibolite from the Median Segment of the Idefjorden Terrane, Lilla Edet. (15 hp)
575. Végvári, Fanni, 2019: Vulkanisk inverkan på klimatet och atmosfärcirkulationen: En litteraturstudie som jämför vulkanism på låg respektive hög latitud. (15 hp)
576. Gustafsson, Jon, 2019: Petrology of platinum-group element mineralization in the Koillismaa intrusion, Finland. (45 hp)
577. Wahlquist, Per, 2019: Undersökning av mindre förkastningar för vattenuttag i sedimentärt berg kring Kingelstad och Tjutebro. (15 hp)
578. Gaitan Valencia, Camilo Esteban, 2019: Unravelling the timing and distribution of Paleoproterozoic dyke swarms in the eastern Kaapvaal Craton, South Africa. (45 hp)
579. Eggert, David, 2019: Using Very-Low-Frequency Electromagnetics (VLF-EM) for geophysical exploration at the Albertine Graben, Uganda - A new CAD approach for 3D data blending. (45 hp)
580. Plan, Anders, 2020: Resolving temporal links between the Högberget granite and the Wigström tungsten skarn deposit in Bergslagen (Sweden) using trace elements and U-Pb LA-ICPMS on complex zircons. (45 hp)
581. Pilsner, Hannes, 2020: A geophysical survey in the Chocaya Basin in the central Valley of Cochabamba, Bolivia, using ERT and TEM. (45 hp)
582. Leopardi, Dino, 2020: Temporal and genetical constraints of the Cu-Co VenaDampetorp deposit, Bergslagen, Sweden. (45 hp)
583. Lagerstam Lorient, Clarence, 2020: Neck mobility versus mode of locomotion – in what way did neck length affect swimming performance among Mesozoic plesiosaurs (Reptilia, Sauropterygia)? (45 hp)
584. Davies, James, 2020: Geochronology of gneisses adjacent to the Mylonite Zone in southwestern Sweden: evidence of a tectonic window? (45 hp)
585. Foyn, Alex, 2020: Foreland evolution of Blåisen, Norway, over the course of an ablation season. (45 hp)
586. van Wees, Roos, 2020: Combining luminescence dating and sedimentary analysis to derive the landscape dynamics of the Velická Valley in the High Tatra Mountains, Slovakia. (45 hp)
587. Rettig, Lukas, 2020: Implications of a rapidly thinning ice-margin for annual moraine formation at Gornergletscher, Switzerland. (45 hp)
588. Bejarano Arias, Ingrid, 2020: Determination of depositional environment and luminescence dating of Pleistocene deposits in the Biely Váh valley, southern foothills of the Tatra Mountains, Slovakia. (45 hp)
589. Olla, Daniel, 2020: Petrografisk beskrivning av Prekambriska ortognejser i den undre delen av Särsvskollan, mellersta delen av Skollenheten, Kaledonska orogenen. (15 hp)
590. Friberg, Nils, 2020: Är den sydatlantiska magnetiska anomalin ett återkommande fenomen? (15 hp)
591. Brakebusch, Linus, 2020: Klimat och väder i Nordatlanten-regionen under det senaste årtusendet. (15 hp)
592. Boestam, Max, 2020: Stränder med erosion och ackumulation längs kuststräckan Trelleborg - Abbekås under perioden 2007 -2018. (15 hp)
593. Agudelo Motta, Laura Catalina, 2020: Methods for rockfall risk assessment and estimation of runout zones: A case study in Gothenburg, SW Sweden. (45 hp)
594. Johansson, Jonna, 2020: Potentiella nedslagskratrar i Sverige med fokus på Östersjön och östkusten. (15 hp)
595. Haag, Vendela, 2020: Studying magmatic systems through chemical analyses on clinopyroxene - a look into the history of the Teno ankaramites, Tenerife. (45 hp)
596. Kryffin, Isidora, 2020: Kan benceller bevaras över miljontals år? (15 hp)
597. Halvarsson, Ellinor, 2020: Sökande efter nedslagskratrar i Sverige, med fokus på avtryck i berggrunden. (15 hp)
598. Jirdén, Elin, 2020: Kustprocesser i Arktis – med en fallstudie på Prins Karls Forland, Svalbard. (15 hp)
599. Chonewicz, Julia, 2020: The Eemian Baltic Sea hydrography and paleoenvironment based on foraminiferal geochemistry. (45 hp)
600. Paradeisis-Stathis, Savvas, 2020: Holocene lake-level changes in the Siljan Lake District – Towards validation of von Post's

- drainage scenario. (45 hp)
601. Johansson, Adam, 2020: Groundwater flow modelling to address hydrogeological response of a contaminated site to remediation measures at Hjortsberga, southern Sweden. (15 hp)
602. Barrett, Aodhan, 2020: Major and trace element geochemical analysis of norites in the Hakefjorden Complex to constrain magma source and magma plumbing systems. (45 hp)
603. Viðarsdóttir, Halla Margrét, 2020: "Man fyller det med information helt enkelt": en fenomenografisk studie om studenters upplevelse av geologisk tid. (45 hp)
604. Zachén, Gabriel, 2020: Classification of four mesosiderites and implications for their formation. (45 hp)
605. Viðarsdóttir, Halla Margrét, 2020: Assessing the biodiversity crisis within the Triassic-Jurassic boundary interval using redox sensitive trace metals and stable carbon isotope geochemistry. (45 hp)
606. Tan, Brian, 2020: Nordvästra Skånes prekambriiska geologiska utveckling. (15 hp)
607. Taxopoulou, Maria Eleni, 2020: Metamorphic micro-textures and mineral assemblages in orthogneisses in NW Skåne – how do they correlate with technical properties? (45 hp)
608. Damber, Maja, 2020: A palaeoecological study of the establishment of beech forest in Söderåsen National Park, southern Sweden. (45 hp)
609. Karastergios, Stylianos, 2020: Characterization of mineral parageneses and metamorphic textures in eclogite- to highpressure granulite-facies marble at Allmenningen, Roan, western Norway. (45 hp)
610. Lindberg Skutsjö, Love, 2021: Geologiska och hydrogeologiska tolkningar av SkyTEM-data från Vombsänkan, Sjöbo kommun, Skåne. (15 hp)
611. Hertzman, Hanna, 2021: Odensjön - A new varved lake sediment record from southern Sweden. (45 hp)
612. Molin, Emmy, 2021: Rare terrestrial vertebrate remains from the Pliensbachian (Lower Jurassic) Hasle Formation on the Island of Bornholm, Denmark. (45 hp)
613. Höjbert, Karl, 2021: Dendrokronologi - en nyckelmetod för att förstå klimat- och miljöförändringar i Jämtland under holocen. (15 hp)
614. Lundgren Sassner, Lykke, 2021: A Method for Evaluating and Mapping Terrestrial Deposition and Preservation Potential- for Palaeostorm Surge Traces. Remote Mapping of the Coast of Scania, Blekinge and Halland, in Southern Sweden, with a Field Study at Dalköpinge Ängar, Trelleborg. (45 hp)
615. Granbom, Johanna, 2021: En detaljerad undersökning av den mellanordoviciska "furudalkalkstenen" i Dalarna. (15 hp)
616. Greiff, Johannes, 2021: Oolites from the Arabian platform: Archives for the aftermath of the end-Triassic mass extinction. (45 hp)
617. Ekström, Christian, 2021: Rödfärgade utfällningar i dammanläggningar orsakade av *G. ferruginea* och *L. ochracea* - Problemstatistik och mikrobiella levnadsförutsättningar. (15 hp)
618. Östsjö, Martina, 2021: Geologins betydelse i samhället och ett första steg mot en geopark på Gotland. (15 hp)
619. Westberg, Märta, 2021: The preservation of cells in biomineralized vertebrate tissues of Mesozoic age – examples from a Cretaceous mosasaur (Reptilia, Mosasauridae). (45 hp)
620. Gleisner, Lovisa, 2021: En detaljerad undersökning av kalkstenslager i den mellanordoviciska gullhögenformationen på Billingen i Västergötland. (15 hp)
621. Bonnevier Wallstedt, Ida, 2021: Origin and early evolution of isopods - exploring morphology, ecology and systematics. (15 hp)
622. Selezeneva, Natalia, 2021: Indications for solar storms during the Last Glacial Maximum in the NGRIP ice core. (45 hp)
623. Bakker, Aron, 2021: Geological characterisation of geophysical lineaments as part of the expanded site descriptive model around the planned repository site for high-level nuclear waste, Forsmark, Sweden. (45 hp)



LUNDS UNIVERSITET

Geologiska institutionen
Lunds universitet
Sölvegatan 12, 223 62 Lund